NASA Contractor Report 189591

Analysis of Rotor Vibratory Loads Using Higher Harmonic Pitch Control

Todd R. Quackenbush
Donald B. Bliss
Alexander H. Boschitsch
Daniel A. Wachspress

CONTINUUM DYNAMICS, INC.
Princeton, New Jersey

CONTRACT NAS1-19160
April 1992

National Aeronautics and
Space Administration

Langley Research Center
Hampton, Virginia 23665-5225

ABSTRACT

Experimental studies of isolated rotors in forward flight have indicated considerable potential for noise reduction through the application of higher harmonic pitch control. Tests to date also show that such pitch inputs can also generate substantial vibratory loads. This report summarizes the modification of the RotorCRAFT (Computation of Rotor Aerodynamics in Forward Flight) comprehensive analysis of isolated rotors to study the vibratory loading generated by representative high frequency pitch inputs. The RotorCRAFT code has been developed for use in the computation of such loading, and incorporates a highly refined rotor wake model to facilitate this task. This model discretizes the sheet of vorticity that trails from each blade by laying out vortex filaments along contours of constant sheet strength. In previous work this Constant Vorticity Contour (CVC) wake model has been found to be an important contributor to improved accuracy in the prediction of unsteady airloads. This report describes the extension of RotorCRAFT to include a variety of features needed for the study of vibratory response to higher harmonic pitch, blade/vortex interaction events, and the prediction of rotor noise. These include: application of arbitrary root pitch control; computation of internal blade stresses and hub loads; improved modeling of near wake unsteady effects; and preliminary implementation of a coupled prediction of rotor airloads and noise. Correlation studies are carried out with existing blade stress and vibratory hub load data. Sample calculations are executed to illustrate the capabilities of the modified RotorCRAFT code and to point out possible directions for future work.

TABLE OF CONTENTS

NOMENCLATURE

A	array of vortex lattice influence coefficients
c	blade chord
[D]	diagonal matrix with components, { ω_i^2 GM(i) }
dT/dr	thrust force distribution along the span (shaft axis)
E	Young's modulus
$\vec{F}$	vector of hub forces in the shaft frame (H,Y,T)
$\{F^{aero}\}$	vector of nodal forces due to aerodynamic loading
$F^{AERO}(i)$	i-th modal force due to aerodynamic forces defined in Equation 3.26c
$\{F^{AEROC}\}$	contribution of aerodynamic forces to $\{F_c\}$ defined in Equations 3.35c and 3.37
$\{F_c\}$	constraint force vector defined in Equation 3.27
$\{F^{rot}\}$	vector of nodal forces due to blade rotation
$F^{ROT}(i)$	i-th modal force due to blade rotation forces defined in Equation 3.26d
$\{F^{ROTC}\}$	contribution of blade rotation forces to $\{F_c\}$ defined in Equation 3.35d
G	shear modulus
$\vec{g}$	vector of vortex lattice circulation values
GM(i)	generalized mass corresponding to mode, i, defined in Equation 3.26a
$\vec{I}_s, \vec{J}_s, \vec{K}_s$	unit vectors of the shaft reference frame
$\vec{i}, \vec{j}$	unit vectors parallel and perpendicular to the blade span
[K]	rotor blade stiffness matrix
K	finite element stiffness matrix
K_{cc}	partition of stiffness matrix corresponding to the constrained degrees of freedom
K_{cr}, K_{rc}	partition of stiffness matrix with rows corresponding to the constrained degrees of freedom, and columns corresponding the remaining free degrees of freedom; and its transpose respectively
$K_{c\theta_c}$	column vector of K_{cc} corresponding to the root twist displacement
K_{rr}	partition of stiffness matrix with rows and columns corresponding to constrained degrees of freedom, deleted
$K_{r\theta_c}$	column of the stiffness matrix associated with the root twist

ℓ	length of finite element
M	finite element mass matrix
[M]	rotor blade mass matrix
$\vec{M}$	vector of hub moments in the shaft frame
{MCYC}	inertia term determining contribution of cyclic pitch acceleration to $\{F_c\}$ defined in Equation 3.35b
M_{cc}, M_{cr}, M_{rc}, M_{rr}	analogous definitions as for K_{cc}, K_{cr}, K_{rc}, K_{rr} applied to the mass matrix
$M_{c\theta_c}$	column vector of M_{cc} corresponding to the root twist displacement
[MFC]	vector of inertia terms determining contribution of modal acceleration vector to $\{F_c\}$ defined in Equation 3.35a
$M_{r\theta_c}$	column of the mass matrix associated with the root twist
MRC(i)	modal mass associated with cyclic pitch for mode, i, defined in Equation 3.26e
$\vec{n}$	normal vector at vortex lattice control points
$\vec{q}$	flow field velocity vector
$\{q\}$	vector of generalized finite element nodal deformations
$\{q\}_r$	vector of generalized finite element nodal displacements
q_i	components of $\{q\}$
$\{\tilde{q}^{rot}\}$	residual displacement vector defined in Equation 3.41
$\{q^{rot}\}$	vector of generalized displacements due to blade rotation forces defined in Equation 3.42
r	radial distance from rotor hub
r_c	vortex core radius
$\{r_{\theta_c}\}$	vector of generalized rigid body displacements due unit cyclic pitch defined in Equations 3.19 and 3.20
r_v	radial location of vortex release point
R	rotor radius
R_X, R_Y, R_Z	rotations due to deformation about the global XYZ axes respectively
s	nondimensional time ($U_{ref}t/c$)
s_T	nondimensional time step for one azimuthal increment
SIGXX(nm,ir,k)	array of axial stress vector contributions for mode, nm, at radial location, ir, defined in Equations 3.46 and 3.50
$[T_{GL}]$	matrix relating local finite element displacement vector to the corresponding global quantities

$[T_{rot}]$	transformation matrix relating axes local finite element axes xyz and rotating blade axes XYZ defined in Equation 3.1
u(x)	local finite element extension deformation at x
U	displacement along global X-axis
U_{ref}	reference velocity for nondimensional time
v_θ	vortex swirl velocity
v(x),w(x)	local finite element transverse displacements at x in the local y and z directions respectively
w, $\vec{w}$	downwash at blade control points
V,W	displacements along global Y and Z axes respectively
xyz	local axes for a finite element
$\{x_i\}$	eigenvector corresponding to modal frequency, ω_i obtained by solving Equation 3.23
[X]	matrix of column vectors, $\{x_i\}$
XYZ	rotating blade coordinates
$X_0Y_0Z_0$	XYZ position of the origin of local finite element axes

β	angle between the local y and η axes
ε_{xx}	axial strain defined in Equation 3.8a
$\varepsilon_{x\eta}$, $\varepsilon_{x\zeta}$	strain tensors defined in Equation 3.8
$\vec{\gamma}$	vector vorticity field in the rotor wake
$\gamma_{x\eta}$, $\gamma_{x\zeta}$	engineering shear strains defined in Equation 3.8
Γ	bound circulation on the blade
η, ζ	principal axes of the cross-section
$\{\eta\}$	vector of modal amplitudes defined in Equation 3.24
$\Phi(\ )$	components of indicial function for downwash
$\{\Phi_2\},\{\Phi_3\}$	vector of shape functions defined in Equation 3.4
ρ	air density
ρ_v	radial distance from vortex center
σ_{xx}	axial stress defined in Equation 3.13a
$\sigma_{xx}(nm)$	contribution of nm-th mode to the axial stress
$\sigma_{x\eta}$, $\sigma_{x\zeta}$	shear stresses defined in Equation 3.13
$\theta(x)$	local twist displacement of finite element
θ_c	cyclic pitch displacement

ψ	azimuth angle of rotor blade
ψ_c	phase angle of higher harmonic pitch input
$\Psi(x,\eta,\zeta)$	Saint Venant warping function relating out-of-plane warping to torsional displacement defined in Equation 3.10
ω_i	natural frequency of i-th mode obtained by solving Equation 3.23
Ω	rotor rotation frequency
ξ	normalized coordinate, x/ℓ

$(\bullet)_G$, $(\bullet)_L$	refers to global axes and local axes respectively
$(\bullet)_{ie}$	refers to element, ie
$(\bullet)_{,x}$	derivative w.r.t. x
$(\bullet)^T$	transpose operation
$()'$	derivative w.r.t. ξ
$(\dot{\bullet})$	derivative w.r.t. time

1. INTRODUCTION

Efforts to predict and reduce the noise generated by helicopter rotors have been underway for several decades. Recent experiments (Ref. 1) have suggested that application of higher harmonic pitch control holds substantial promise as a technique for reducing the noise due to wake/blade interaction. However, results to date have also indicated that substantial vibratory loads can be generated as a consequence of such inputs, and it was judged important to understand the potential tradeoffs between possible noise reductions and increased vibration.

To support the ongoing work in this area, the aerodynamic loading model in the RotorCRAFT (Computation of Rotor Aerodynamics in Forward flighT) free wake analysis of rotors in forward flight has been extensively modified and a wide range of demonstration calculations undertaken. Earlier work (Ref. 2) centered on the development of the Mod 0.0 version of RotorCRAFT, a comprehensive analysis of rotor aerodynamic loading in forward flight using an advanced model of the vortex wake. The overall goal of the present effort was to enhance the capabilities of the baseline code to permit the computation of blade stresses and hub loads due to higher harmonic pitch inputs. As will be described below, this involved not only a substantial extension of the original structural model but also refinements in the modeling of unsteady loads generated by the near wake. Also, new output features have been added to permit the visualization of wake-induced velocity fields and the generation of unsteady airloads in a format suitable for input to NASA's WOPWOP code. The latter feature is present in a preliminary form only, however, and is suitable primarily for demonstration calculations of noise, not for data correlation efforts. A separate effort is presently underway to develop new, more efficient and accurate noise calculations.

The RotorCRAFT code features unique capabilities that were judged to make a suitable platform for the research and correlation effort undertaken here. Among these is the Constant Vorticity Contour (CVC) wake model implemented in the code, a novel discretization of the wake into filamentary vortices representing constant-strength contours of vorticity in the vortex sheets that trail from each blade. The CVC model is noteworthy in that it eliminates the artificial distinction between vorticity generated by azimuthal and spanwise changes in the bound circulation on the blade (i.e., between what is conventionally termed "shed" and "trailed" vorticity) and in that it provides a visually meaningful representation of the wake. Previous work (Refs. 2-5) has indicated the success of this approach for obtaining improved predictions of wake-induced vibratory airloads relative to more simplified models using, for example, a single tip vortex.

The computation of aerodynamic loads in the presence of the wake-induced flow field is carried out in the present analysis using a vortex lattice model of the blade. This model is appropriate for rotor calculations because of its potential for refined treatment of tip effects and wake/blade interaction. As will be described below, the development of the Mod 1.0 variant has also involved studies of an improved model of unsteady near-wake aerodynamic loading, a feature that can be important for handling cases involving higher harmonic pitch control. Similarly, in cases involving high frequency pitch forcing, an appropriate treatment of the dynamics of the rotor blade is particularly important. The present report documents the extension of the finite element model of structural deflection originally described in Reference 2 to the problem of the prediction of internal blade stresses as well as forces and moments on the rotor hub.

Finally, the results presented here include correlation studies of predicted rotor hub loads from the data available in Reference 1 as well as additional data from the literature on rotor blade stress computations. These correlations will be discussed after the presentation of information on the development of the present model in the next three sections.

2. BACKGROUND ON THE ROTORCRAFT AERODYNAMIC MODEL

A detailed discussion of the development of the baseline aerodynamic model is presented in Reference 2. This section briefly summarizes the major features of the technical background of the code. Before presenting this discussion, it is appropriate to briefly review past work on forward flight airloads in the literature.

Scully (Ref. 6) developed a free wake analysis of the rotor using two free filaments (a rolled-up tip vortex and a diffuse inboard filament) to model the rotor wake. This distorted wake model succeeded in predicting certain features of the unsteady loading on rotors, though uncertainties about the proper modeling of close blade/wake interactions precluded accurate prediction of higher harmonic loads. Other broadly similar wake models have been developed over the last fifteen years (Refs. 7-9). The seminal paper of Hooper (Ref. 10) pointed out the inadequacy of these types of models in predicting the nearly impulsive airloading events that occur in a broad range of rotor designs, particularly in high speed flight. His results suggested that some aspects of the traditional approach to rotor wake aerodynamics must be inadequate, at least for the high speed case. Recent work by Miller and (Ref. 11) and Johnson (Ref. 12) has been directed toward repairing some of the shortcomings in previous single-tip-vortex models. Hooper's results also motivated the development of the CVC model into a comprehensive free wake model suitable for application to rotors at both low and high forward speeds. The following sections describe the foundations of the CVC model and the methods used to incorporate it into the RotorCRAFT rotor analysis code.

2.1 Constant Vorticity Contour (CVC) Rotor Wake Model

The CVC method uses the curved vortex elements described in References 2, 13, and 14 as the fundamental building blocks of a free wake model. The use of these elements contributes substantially to the accuracy and efficiency of the wake model and is particularly effective for representing the complex wake characteristics of forward flight. These complexities arise because the time-varying loading experienced by rotor blades generates both trailed and shed vorticity components in the wake. An idealized sequence of advancing side load distributions containing this behavior is sketched in Figure 2-1. A corresponding sequence of bound circulation distributions would exhibit similar behavior. Spanwise variations in the bound circulation are responsible for the "trailed" component of wake vorticity and temporal (i.e, azimuthal) variations are responsible for the "shed" component. Given a bound circulation distribution along the span, $\Gamma(r,\psi)$, the wake that trails from the blade consists of a continuous sheet of vorticity whose strength as it leaves the blade is $\gamma(r,\psi)$. This can be represented by

$$\vec{\gamma} = \gamma_s \hat{i} + \gamma_c \hat{j} \tag{2.1}$$

where s and c are defined parallel to the span and to the chord of the blade, respectively. The intensity of each component of vorticity is related to the bound circulation by

$$\gamma_s = \frac{-\partial\Gamma(r,\psi)}{\partial t} \tag{2.2}$$

and

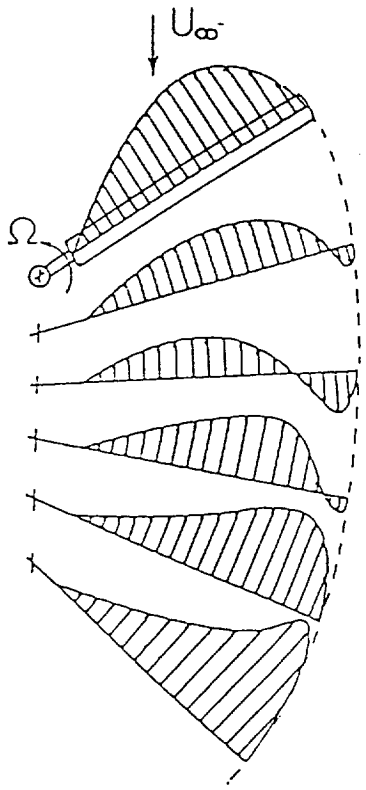

Figure 2-1. Typical load variations on the advancing side in high speed flight.

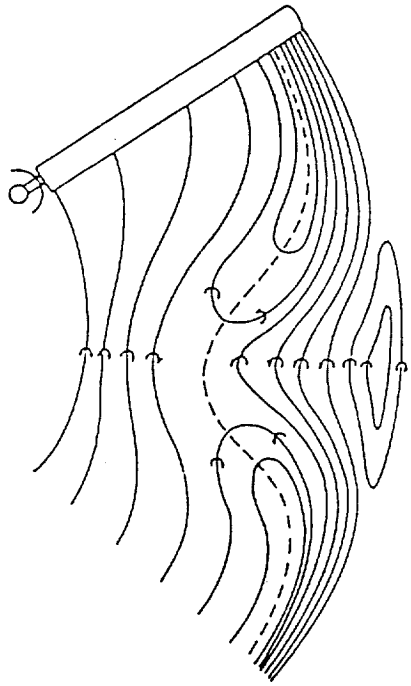

Figure 2-2. Contours of constant sheet strength in the wake on the advancing side.

$$\gamma_c = \frac{-\partial\Gamma(r,\psi)}{\partial r} \tag{2.3}$$

while the magnitude of the vector is determined by

$$\gamma = \left|\vec{\gamma}\right| = \sqrt{\gamma_s^2 + \gamma_c^2} \tag{2.4}$$

Note that the strength of the wake sheet may be zero and that each component may reverse sign depending on the strength and rate of change (spatial or temporal) of the bound circulation.

Figure 2-2 shows the idealized wake vorticity field corresponding to the load variations in Figure 2-1. The wake here is shown in terms of contours of constant sheet strength, i.e. lines of constant γ are depicted (ignoring any vertical distortion). Clearly, only a finite number of contour lines are used in this figure, though a continuum of lines are in fact required to completely represent the wake sheet. Because increments in γ are constant between each contour line, the amount of circulation contained between any two contour lines on the sheet is constant. This increment in circulation is related to the bound circulation on the blade as follows:

$$\Delta\Gamma = \int_r^{r+\Delta r} -\gamma(r,\psi)\, dr = \Gamma(r+\Delta r,\psi) - \Gamma(r,\psi) \tag{2.5}$$

If the origination points of contour lines (denoted "release points") are spaced radially along the blade corresponding to fixed increments in bound circulation, then the radial distance between the contour lines will be a direct measure of the gradient in bound circulation along the blade. That is, if $\Delta\Gamma$ is held constant, the approximate relationship

$$\frac{\partial\Gamma(r,\psi)}{\partial r} \cong \frac{\Delta\Gamma}{\Delta r(r,\psi)} \tag{2.6}$$

means that the contour spacing will be inversely proportional to the spanwise circulation gradient. Thus, contour lines will be tightly spaced in the radial direction where gradients of bound circulation are high, as is typically true near the blade tip at most azimuth angles. As Figure 1 makes clear, however, realistic blade load variations do not always produce large bound circulation gradients near the blade tips. Gradients are often shallow at the advancing tip in high speed flight, and so the wake may take on a more sheet-like character, rather than rolling up into a concentrated tip vortex. Conversely, bound circulation gradients may not always be shallow in certain regions. Note in particular that the radial gradients near the blade root in forward flight may be relatively large compared to the weak gradients typically seen in the inboard loading distribution of hovering rotors. Thus, unlike the diffuse inboard wakes usually present on rotors in hover, concentrated vortical structures may be present trailing from the root region of rotors in high speed flight.

Note that the tangent to the contour line at any point determines the direction of the local vorticity vector $\vec{\gamma}$, with the "trailed" and "shed" vorticity simply being components of the resultant vector $\vec{\gamma}$. While conceptually convenient to retain this terminology in some cases, it is desirable to employ a wake discretization that removes the artificial distinction between these two quantities and treats the vector vorticity field in a unified manner. The first step in constructing such a discretization is to recall that the contour lines can in fact be treated as vortex filaments. The natural step to take in representing the wake is thus to lay down curved vortex elements along the contours of constant wake strength, as shown in Figure 2-3. To conserve circulation in the wake, these filaments are assumed to contain all of the rolled-up vorticity trailed between adjacent release points. This means that all of the filaments will have equal strength $\Delta\Gamma$, and the filaments have constant strength along their length.

The shed and trailed vorticity is thus accounted for by the fact that the direction of the tangent vector to the resultant elements changes continuously even though the strength of each filament is constant. Using the CVC approach, on the average only half as many elements are required as in the straight-line lattice method, where the local vorticity vector is represented by two discrete straight elements. Thus, the use of curved elements means that fewer, relatively large elements can be used to accurately represent the vector vorticity field in the wake. These factors give the full-span CVC wake model a substantial advantage in efficiency relative to the lattice approach; since the model requires roughly half the number of elements, the number of operations required to compute the wake-on-wake velocity field will be reduced by approximately a factor of four.

As noted above, by choosing each contour filament to be of equal strength the filaments are closely spaced in regions of high circulation, and are widely spaced in regions where the circulation is low. This relationship between filament spacing and sheet strength, and the fact that the filaments follow the actual vortex lines, means that the structure and relative strength of the wake can be seen visually. Since the computational filaments are aligned along the true vortex lines in the wake, this seems to be the most natural and accurate representation of the wake. Also, because the "shed" cross-filaments present in the lattice model are eliminated, an additional discretization along the wake length is not needed and the potential problems of handling these cross-filaments in a free wake representation are avoided.

Once the wake is laid out, its spatial evolution proceeds in the same way as in traditional Lagrangian models. The key difference is that the wake now trails from the full span of the blade and is not a simple root/tip filament pair. Calculations discussed in Reference 3 have shown the important role played by the wake of the inboard portion of the blade. In addition, this full-span approach naturally allows for the appearance, evolution, and disappearance of the wake of opposite-sign circulation zones (e.g., near the tip) as they occur. Two new features of the wake representation that must be addressed are the formation of loops in the wake and the spanwise variation in filament release points as the blade rotates. Handling both of these features requires careful treatment of the numerical logic involved in filament generation and amalgamation. Current procedures in RotorCRAFT have proved robust in this respect.

In its current form, the analysis starts with an estimate of the spanwise bound circulation distribution at a set of azimuthal locations, computed using a vortex lattice treatment of the blade loading in conjunction with a simple uniform inflow model. The spanwise release points for the individual discrete filaments are found by interpolation

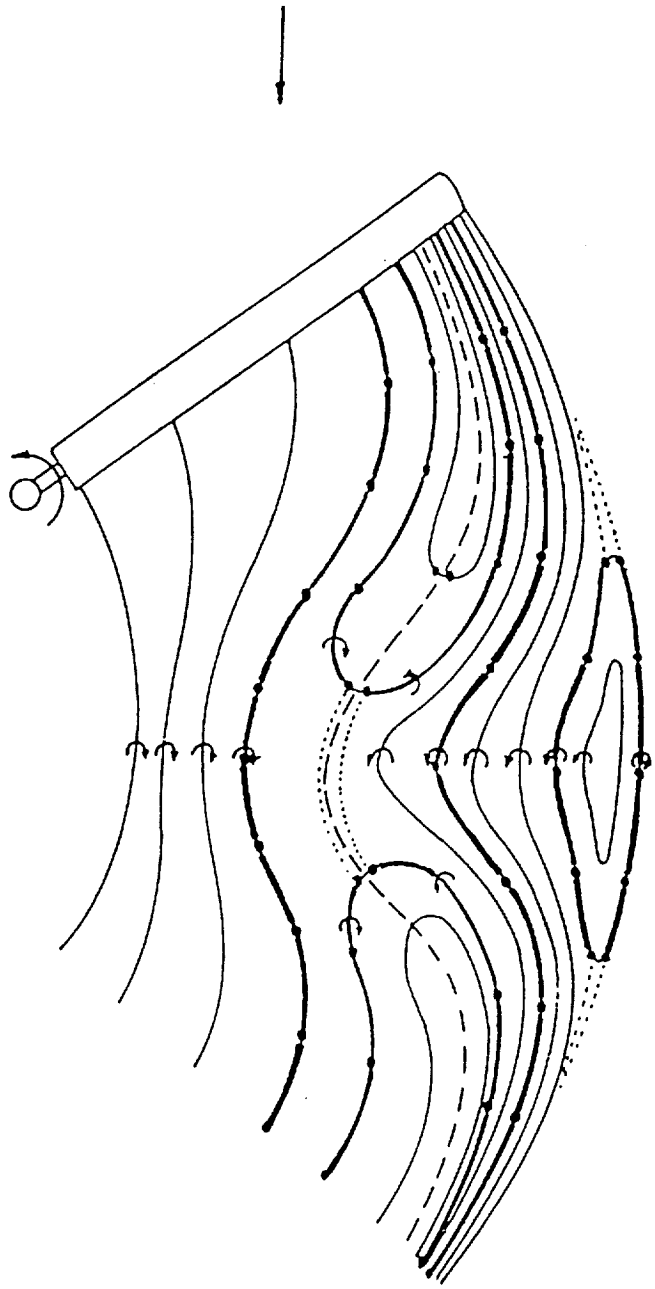

Figure 2-3. Modeling the wake structure with curved vortex elements.

between the fixed calculation points along the span. This must be done at each azimuthal station since the circulation distribution changes. Not only do the release points shift along the blade span but some of them also disappear and reappear as the maximum circulation decreases and increases. This disappearance and reappearance corresponds to the formation of loops in the wake.

Although the use of the full-span CVC wake model is important to the computation of wake motion and wake-induced velocities in the region near the rotor, it is in general computationally inefficient to retain this model over the full length of a semi-infinite wake. Thus, provision has been made for using a set of successively simpler wake models that are invoked for regions far from the rotor disk. Reference 2 discusses the steps taken to allow efficient far wake modeling in detail. This reference and the RotorCRAFT Users Manual (Ref. 15) also describe the technical background of the present vortex core model as well as guidelines for its implementation.

2.2 Flow Field Calculations

As noted above, the Mod 0.0 version of RotorCRAFT was intended primarily as a tool to investigate unsteady airloading on rotors in forward flight. The role played by the wake-induced velocity field in such calculations is, of course, critical. RotorCRAFT (Mod 0.0) allows for printing out the velocity induced at the control points of the vortex lattice, though it does not provide for evaluation of wake-induced flow fields at other points of evaluation. Such a capability is potentially very useful for analyzing important effects involving blade/vortex interactions, as well as for visualization of wake behavior. Thus, as described in Reference 15, users of RotorCRAFT (Mod 1.0) may select as many as 1200 evaluation points off the rotor disk where the wake-induced velocity will be computed and printed out. These points are typically arranged in 'scan planes', and the present implementation allows for as many as three separate scan planes containing 400 points.

Figure 2-4 shows typical output produced using this capability. It illustrates two views of the instantaneous flow field in the vicinity of a UH-60 rotor in forward flight at advance ratio 0.3 and thrust coefficient 0.007. Figure 2-4a shows a top view of the rotor disk with a contour plot of the downwash contours in a plane normal to the rotor shaft and 0.1R above the hub. (This particular rendering is in black and white, but much more instructive plots can be done in color with any number of current software packages). This plot shows many of the expected flow features associated with a typical rotor's aerodynamic environment: a region of upwash near the front edge of the disk; a relatively large region of downwash in the first quadrant, downstream of the advancing side; steep velocity gradients near the edges of the disk, with the wake downstream of the advancing tip being more diffuse than that on the retreating side; and an area of relatively quiescent flow on the retreating side near the hub. Figure 2-4b shows a vector plot of the crossflow downstream of the same rotor, showing the expected swirling flow associated with the two tip vortices as well as a crossflow component on the inboard portion of the advancing side. These figures are merely illustrations of the capabilities present in RotorCRAFT (Mod 1.0); more detailed examinations of particular regions of the vortex wake can be found in References 16 and 17.

2.3 Vortex Lattice Blade Model

Many modern rotors feature complex planforms, and it is advantageous to use lifting surface analyses (a subset of aerodynamic panel methods) to analyze such designs. The particular model employed here focuses primarily on thin lifting surfaces with no side- or leading-edge separation (with the exception of tip effects in yawed flow discussed in Ref. 2). This is in the tradition of vortex lattice models first developed by Falkner (Ref. 18) and later

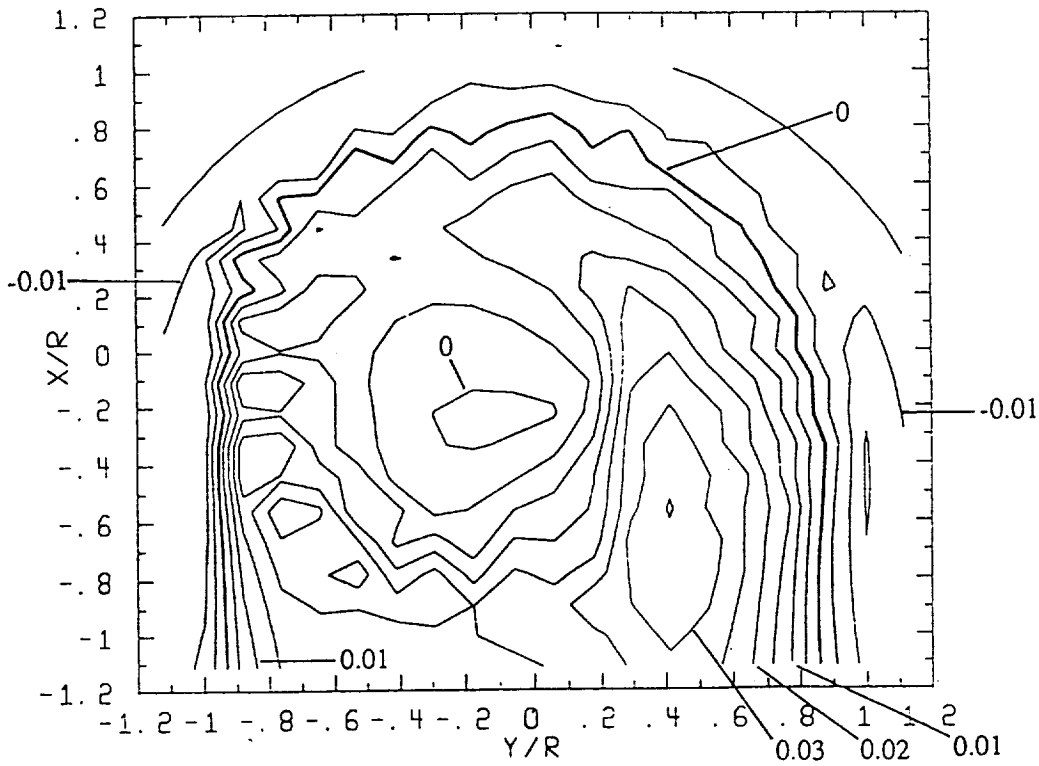

a) Contour plot of downwash in a plane 0.1R above the rotor

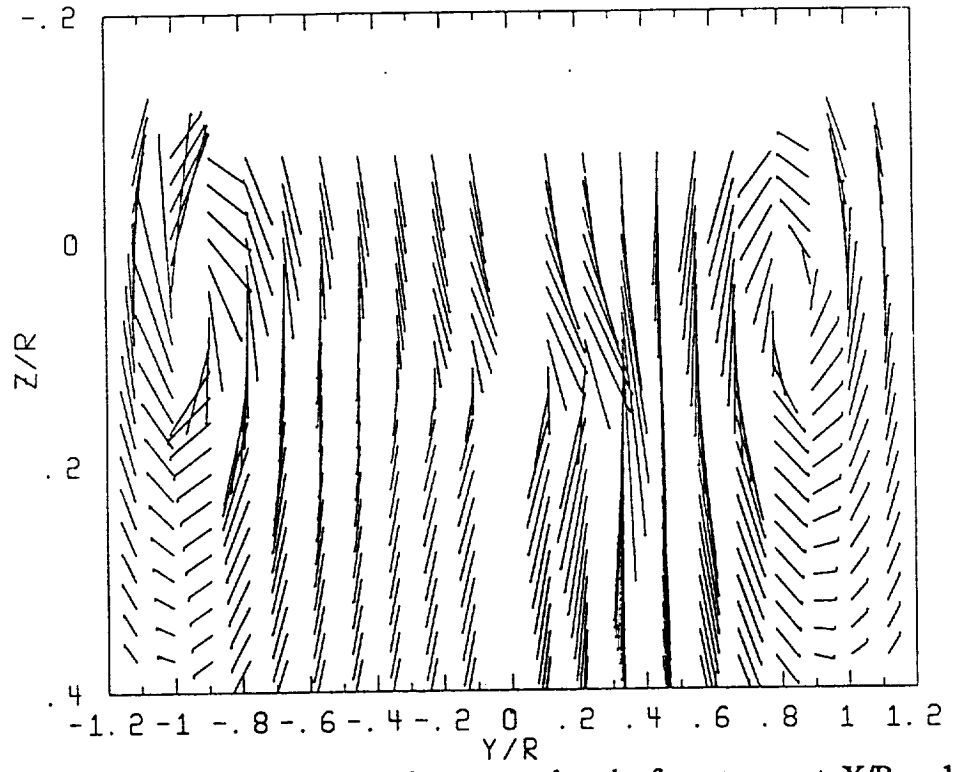

b) Crossflow velocity in a plane normal to the free stream at X/R = -1.0

Figure 2-4. Evaluation of induced velocities in the vicinity of a UH-60 rotor at advance ratio 0.3 and thrust coefficient .007 .

popularized by such researchers as Rubbert (Ref. 19) and Margason and Lamar (Ref. 20). The rotor blade is represented in the present work by a surface consisting of vortex quadrilaterals. Four constant strength straight-line vortices form the sides of each quadrilateral, except at the trailing edge of the blade where a modified vortex quadrilateral without the downstream line vortex is used. Also, as noted above, special modifications can be made to the side edge of the tip in cases where yawed flow causes part of the wake to be trailed from this edge.

The lifting surface/vortex lattice analysis used here was adapted for use from the hover simulation described in Reference 21. This formulation allows substantial flexibility in the specification of the blade's planform so that complex designs may be accommodated. Currently, the lattice can be divided into as many as ten different regions, with separate linear distributions of twist, taper, and sweep within each. The spacing of the quadrilaterals in a vortex lattice analysis is an important consideration (Ref. 22). The judicious selection of the density, spacing, and orientation of the quadrilaterals can considerably enhance the efficiency and rate of convergence of the blade loading.

The solution method used to find the bound circulation given this lattice is essentially a straightforward implementation of the classical approach described in the literature on lattice methods for fixed wing applications (e.g., Reference 20). Given the location and orientation of each of the quadrilaterals on the blade, the velocity induced by the blade lattice on each of the control points is determined, assuming unit strength for each quadrilateral. Then the resulting velocity is resolved in the normal direction at each control point, yielding an array of influence coefficients relating the vector of bound circulations to the blade-induced downwash, w, at each control point:

$$\vec{w} = A\vec{g} \tag{2.7}$$

where

$$A = \frac{\partial w_i}{\partial g_j} \qquad i, j = 1,....N_Q \tag{2.8}$$

Here, N_Q is the number of vortex quadrilaterals on the blade. Note that the location of each of the quadrilaterals as well as the velocities above are defined in the blade reference system depicted in Figure 2-5.

This array of coefficients is stored and the velocity induced at each control point by the free stream, the blade rotation and deflection (discussed below), and the rotor wake are summed and resolved into 'normal-wash' velocities that are then used to find the vector of bound circulation values on the blade that eliminates any flow normal to the blade surface at the specified control points:

$$A\vec{g} + \vec{q} \cdot \vec{n} = \vec{0} \tag{2.9}$$

$$\vec{g} = -A^{-1} (\vec{q} \cdot \vec{n}) \tag{2.10}$$

The bound circulation can then be used to solve for the forces and moments on each segment of the blade by applying the Joukowsky Law to each of the vortex quadrilaterals. This is summed to yield the total force on each blade in shaft coordinates:

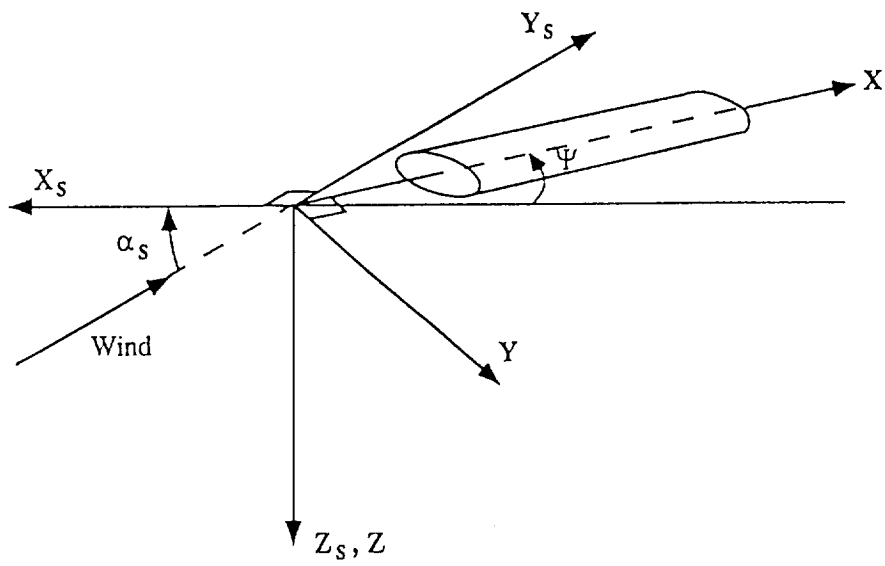

Figure 2-5. Definition of shaft coordinates and blade coordinates.

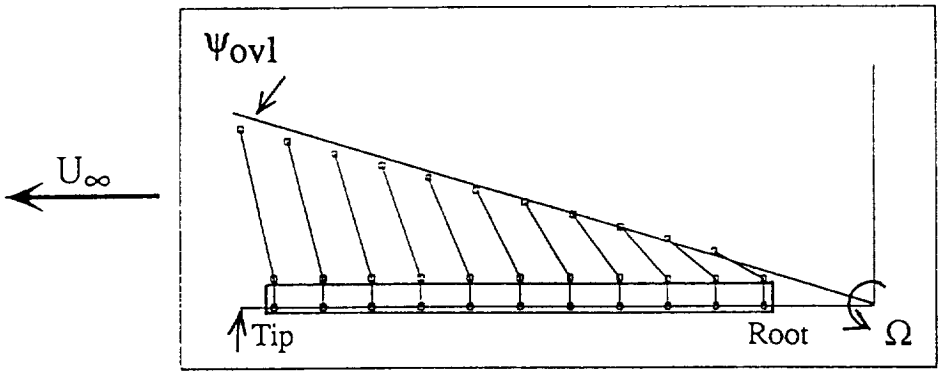

Figure 2-6. Schematic of yawed trailers in the near wake of a rotor blade at $\psi = 0°$, advance ratio 0.4.

$$\vec{F} = \left(H\vec{I}_S + Y\vec{J}_S + T\vec{K}_S\right) = \sum_j \sum_k \vec{F}_{jk} \tag{2.11}$$

Here, j is the summation index over the quadrilaterals on the blade, while k is the index of the blade edges. Moments exerted by the blade about the sectional quarter-chord reference axis can also be computed:

$$\vec{M} = \left(L\vec{I}_S + M\vec{J}_S + N\vec{K}_S\right) = \sum_j \sum_k \vec{F}_{jk} \times \vec{r}_{jk} \tag{2.12}$$

Moments about the flapping and lagging axes of the blade are taken to compute the gross blade motion, while pitching moments can be computed for each section to use for the calculation of torsional deformation. Here, $\vec{r}_{jk}$ is the vector from the reference axis to the point of action of $\vec{F}$. Tabulated information on pitching moment coefficients can also be used to determine the moments, as is described in Reference 2 .

The forces predicted by the basic vortex lattice analysis must be modified to include predictions of viscous drag for performance calculations, as well as the effect of compressibility on the sectional lift and moment. Other modifications are necessary to account for stall, yawed flow, and unsteady effects in the near wake (Ref. 2). To introduce forces generated by profile (viscous and pressure) drag into the calculation, the only practical approach at present is the use of two-dimensional airfoil data. The form of data required for this coupling is tabulated values for sectional drag coefficients as a function of both Mach number and sectional angle of attack.

Compressibility has an important effect on performance for Mach numbers typical of modern rotors. Some of this effect is captured by the inclusion of Mach number dependence in the 2D airfoil data used for profile drag coefficients. However, compressibility also has a significant impact on the lift generated by airfoils at specified angles of attack, and so its influence on thrust and induced power must be considered as well. For two-dimensional thin airfoils, treatments like the Prandtl-Glauert correction to lift curve slope are useful for including compressibility effects. In vortex lattice calculations, transformations that are similar in spirit but more elaborate in detail must be invoked. Currently, a transformation of the blade geometry is used that involves stretching the chord of the blade at a given radial station based on the local Mach number at that section (Ref. 21). The model also accounts approximately for tip relief effects due to airfoil thickness.

2.4 High Frequency Unsteady Airloads

As discussed in Reference 2, the original model of the near wake just downstream of each rotor blade consists of a set of straight vortex trailers that are extended back into the wake from the bound vortices on the blade. The orientation of these trailers may adjust with the local free stream direction at a given radial station (Fig. 2-6), thus providing a coarse approximation of the behavior of the near wake suitable for the resolution of low-frequency loads; however, any other structure of the shed vorticity within this overlap region is neglected. The effect of the shed vorticity in the wake far downstream of the rotor blade is of course captured with the full-span CVC free wake model.

As part of the improvement of the aerodynamic model of the blade carried out for this effort, a more refined treatment of the unsteady loading due to shed vorticity in the near wake has been studied. The approach presently under investigation involves adjusting the downwash used to compute the loads on the vortex lattice with an approximate indicial

function that captures the near wake effects. In principle, the downwash could be adjusted by explicitly including vortex elements in the near wake, laying out components of shed vorticity parallel to the blade span to supplement the trailers shown in Figure 2-6. This approach involves a variety of computational difficulties, including the need to carefully position the discrete shed vorticity as a function of time step, and the necessity to incur a computational penalty associated with retaining high-resolution discrete vortex representations of the wake.

Given this, it was judged desirable to investigate the use of an indicial function to compute the lift response of the rotor blade to the shed vorticity in the near wake. This approach is implemented in the vortex lattice method as part of the calculation of the induced velocity at a control point. Let w represent the downwash at a typical control point due to the influence of the wake and the blade motion. The modification required to take account of near wake unsteady effects can be formulated as a correction to the downwash w ; the resulting quantity w* will be used to compute the bound circulation distribution and can be stated as:

$$w^*(s) = w\,\Phi_{rt}(s, s_T, N) \tag{2.13}$$

where s is the nondimensional time and Φ_{rt} is an indicial function that reduces to 1.0 in the case where near wake shed vorticity is omitted. The nondimensional time here is s=(Ut/c), where the reference velocity U is assumed to be

$$U = \Omega r + U_\infty \sin\psi \tag{2.14}$$

for a given radial position r and azimuth station Ψ, and U_∞ is the free stream velocity. If ψ_{ovl} is the extent of the overlap near wake (Fig. 2-6), then s_T is the nondimensional time required for the blade to traverse one azimuthal increment $\Delta\psi$. T is the time elapsed during one such blade azimuth increment and N is the number of azimuth increments contained within the overlap region.

The indicial function assumes that the downwash at the control point ramps up linearly from zero over the time step T, reaching its full value at that point. The present vortex lattice scheme assumes essentially a step increase in downwash at each time step that does not generate any shed vorticity in the overlap near wake. The indicial function Φ_{rt} is designed to add in the effect of this near wake while also including the effect of its truncation beyond ψ_{ovl} so as not to double-count the wake that is captured by the CVC model.

In the case of the present rotor wake analysis, the downwash is desired at discrete multiples of the time step T (which is assumed to be the ramp time s_T) :

$$w^*(ns_T) = w\,\Phi_{rt}(ns_T, s_T, N) \tag{2.15}$$

The indicial function can be constructed from

$$\Phi_{rt}(0, s_T, N) = 0$$

and

$$\Phi_{rt}(ns_T,s_T,N) = \Phi_0(ns_T,s_T) + \sum_{m=1}^{\infty} \Phi_m(ns_T,s_T,N) \tag{2.16}$$

where

$$\Phi_0(s,s_T) = 0$$

for $s < s_T$ and

$$\Phi_0(s,s_T) = 1 + \frac{1}{s_T} \ln\left(\frac{s-s_T+2}{s+2}\right) \tag{2.17}$$

for $s \geq s_T$. The term Φ_m is determined by a recursion relation

$$\Phi_m(ns_T,s_T,N) = \sum_{k=1}^{n-mN} \left\{\Phi_{m-1}([k+(m-1)N]s_T,s_T,N) - \Phi_{m-1}([k-i+(m-1)N]s_T,s_T,N)\right\} * \Phi_w([n-mN+1-k]s_T,s_T,N) \tag{2.18}$$

for $n > mN$ and

$$\Phi_m(ns_T,s_T,N) = 0$$

for $n \leq mN$. The term Φ_w in Equation 2.18 is given by

$$\Phi_w(s,s_T,N) = 0$$

for $s < s_T$, while the term

$$\Phi_w(s,s_T,N) = \frac{1}{(2N+1)s_T}\left[1 + \frac{1}{s_T}\ln\left(\frac{s-s_T+2}{s+2}\right)\right] - \frac{2}{(2N+1)s_T}\frac{(2s+2+(2N-1)s_T)}{(2s+4+(2N-1)s_T)}\frac{(s-s_T)}{(2s+(2N-1)s_T)} + \frac{2\left(\ln[(s-s_T+2)(2s+2+(2N-1)s_T)] - \ln[2(2N+1)s_T]\right)}{4(s+2)^2 + 4(s+2)(2N-1)s_T + (2N-1)^2 s_T^2} \tag{2.19}$$

accounts for the wake truncation.

The primary effect of this type of indicial function is to introduce a phase delay into the response of the aerodynamic loading while also decreasing the magnitude of the response to a given upwash or blade motion input. This method has undergone preliminary testing and has so far produced qualitatively reasonable results. However, it is has not yet been thoroughly validated and so has not been used in the calculations described below. The present version of RotorCRAFT (Mod 1.0) contains provisions for activating the near wake model when the final version becomes available.

3. BASELINE MODEL OF BLADE DEFORMATION AND MODAL PROPERTIES

The structural properties of the helicopter blade are clearly critical to the evaluation of the response and performance of a helicopter in forward flight. This is particularly true of the study of rotor vibratory hub loads undertaken here. Thus, one of the major efforts within the development of the RotorCRAFT code has been to incorporate a realistic finite element (F.E.) representation of the blade. The primary emphasis of the Mod 0.0 version of RotorCRAFT was to predict unsteady aerodynamic loading that leads to rotor vibration. The pertinent final report, Reference 2, contains a full discussion of the major features of the finite element model and details of the formulation of the dynamic modeling and its capabilities and limitations. As noted above, this present effort involved the implementation of computations of hub loads and blade stresses. Thus, in the discussion that follows the major features of the finite element model shall be concisely reviewed while the enhancements implemented in RotorCRAFT (Mod 1.0) shall be discussed in greater detail. The description of its coupling with the aerodynamic model discussed above is reserved for Section 4. Further description of the inputs required for this portion of the analysis are given in Reference 15.

3.1 Summary of the Finite Element Structural Model of the Helicopter Blade

A fourteen degree-of-freedom finite element (F.E.) model is used to represent the helicopter blade extension, twist and transverse bending displacements. Stiffness and mass properties for each element are computed from the cross-section geometry and material properties supplied by the user. Blade rotation forces and geometric stiffening effects are accounted for in the construction of the elements. The resulting element matrices are then assembled and any constrained d.o.f. eliminated to finally yield global mass and stiffness matrices for the complete blade structure. The approach taken is similar to previous implementations of F.E. methods for rotorcraft applications, such as Reference 23. The resulting mass and stiffness matrices serve as inputs to a generalized eigenvalue problem which is solved by a Jacobi iterative technique to obtain the modal frequencies and shapes for the F.E. model. The modal properties are dependent upon the frequency of blade rotation since the geometric stiffening is proportional to the square of this frequency.

The transfer of information between the structural and the aerodynamic models in RotorCRAFT occurs chiefly via the modal properties of the blade. The mode shapes are used to compute generalized modal forces from the distributed aerodynamic forces, and these modal forces drive the corresponding modal responses. These responses in turn are used in conjunction with the mode shapes to determine the instantaneous displacements and velocities at any point along the blade. Finally, the blade deformations and deformation rates provide the necessary information to update the flow field and aerodynamic forces, as described in the previous section. Hence, one iterates toward a steady state solution where the blade displacements and their rates are constant at each azimuthal location. The remainder of this section contains a brief review of the main features of the F.E. model with greater emphasis placed upon the computation of hub loads and blade stresses.

3.1.1 Blade Geometry

Each of the blade segments defined in the RotorCRAFT blade geometry input is subdivided into structural finite elements in the manner specified by the user. The global axes for the assembled blade are denoted by XYZ in Figure 3-1, which shows the relationship between shaft, wind, and blade axes. Local axes, xyz , are defined for each element such that the x-axis coincides with the elastic axis, or the line of shear centers, of the element. Axes y and z lie in the cross-sectional plane of the element and are related to

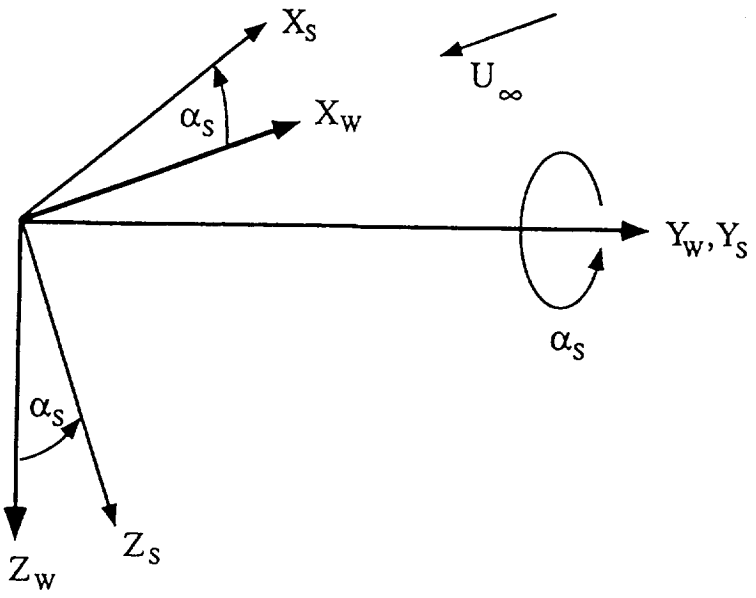

a) Rotation of wind axis system about Y_W to reach shaft axis system (Z_S parallel to rotor shaft)

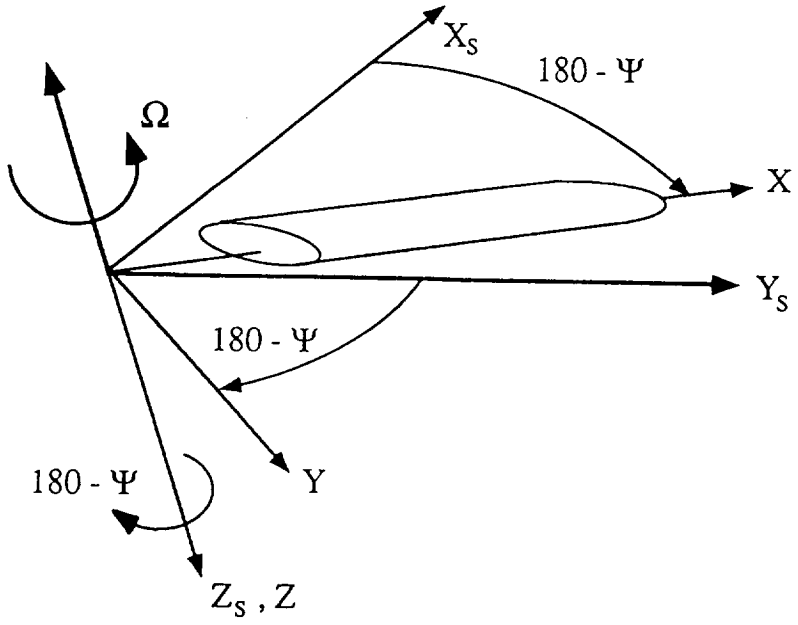

b) Rotation of shaft axes about Z_S to reach blade axis system (X,Y,Z)

Figure 3-1. Axis system definitions.

the global Y and Z axes via a local to global transformation matrix, $[T_{rot}]$. This matrix is constructed from blade segment anhedral, sweep and collective specifications supplied by the user in the blade geometry input file as is explained in Reference 2. The global coordinates, XYZ, of any point on a given F.E. with local coordinates xyz are then given by:

$$\begin{Bmatrix} X \\ Y \\ Z \end{Bmatrix} = \begin{Bmatrix} X_0 \\ Y_0 \\ Z_0 \end{Bmatrix} + [T_{rot}] \begin{Bmatrix} x \\ y \\ z \end{Bmatrix} \tag{3.1}$$

where the coordinates, $X_0Y_0Z_0$, are the global coordinates of the origin of the local axes here taken to lie on the elastic axis at the end of the element nearest the rotor hub. The same transformation matrix is used below in referring local deformations to the global axes. Note that the *rotations* due to deformation can also be referred to the global axes using this transformation since the deformations are assumed small and the associated rotations thus commute.

3.1.2 Element Degrees of Freedom

The specification of the shape functions and the fourteen degrees of freedom of each element is summarized here. Each element has two end nodes and one node at its midpoint, as shown in Figure 3-2. The degrees of freedom correspond to translational and rotational deformations at these nodes. The deformation of the element at any point is estimated by interpolation of the nodal displacements using the shape functions. Let u,v and w denote the displacements along the local x,y, and z axes respectively and θ the twist deformation about the x axis. Then the generalized displacement vector is defined as:

$$\text{Lag:} \quad \begin{Bmatrix} q_1 \\ q_2 \\ q_3 \\ q_4 \end{Bmatrix} = \begin{Bmatrix} v(0) \\ v_{,x}(0) \\ v(\ell) \\ v_{,x}(\ell) \end{Bmatrix}$$

$$\text{Flap:} \quad \begin{Bmatrix} q_5 \\ q_6 \\ q_7 \\ q_8 \end{Bmatrix} = \begin{Bmatrix} w(0) \\ w_{,x}(0) \\ w(\ell) \\ w_{,x}(\ell) \end{Bmatrix}$$

$$\text{Twist:} \quad \begin{Bmatrix} q_9 \\ q_{10} \\ q_{11} \end{Bmatrix} = \begin{Bmatrix} \theta(0) \\ \theta(\ell/2) \\ \theta(\ell) \end{Bmatrix}$$

$$\text{Axial:} \quad \begin{Bmatrix} q_{12} \\ q_{13} \\ q_{14} \end{Bmatrix} = \begin{Bmatrix} u(0) \\ u(\ell/2) \\ u(\ell) \end{Bmatrix} \tag{3.2}$$

where the subscript $(\bullet)_{,x}$ denotes the derivative with respect to the local x axis coordinate and ℓ is the element length. Thus q_1 and q_2 refer to the displacement and corresponding slope due to bending in the y-direction at the left hand node. The corresponding right hand node deformations are q_3 and q_4 , and so forth for the other displacements. Note that the slopes, $v_{,x}$ and $w_{,x}$, can be regarded as a small positive

Local Degrees of Freedom for Blade Element

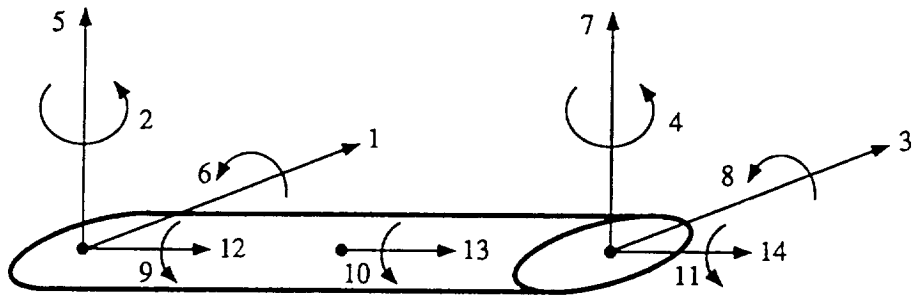

Assembly and Ordering of Global Degrees of Freedom

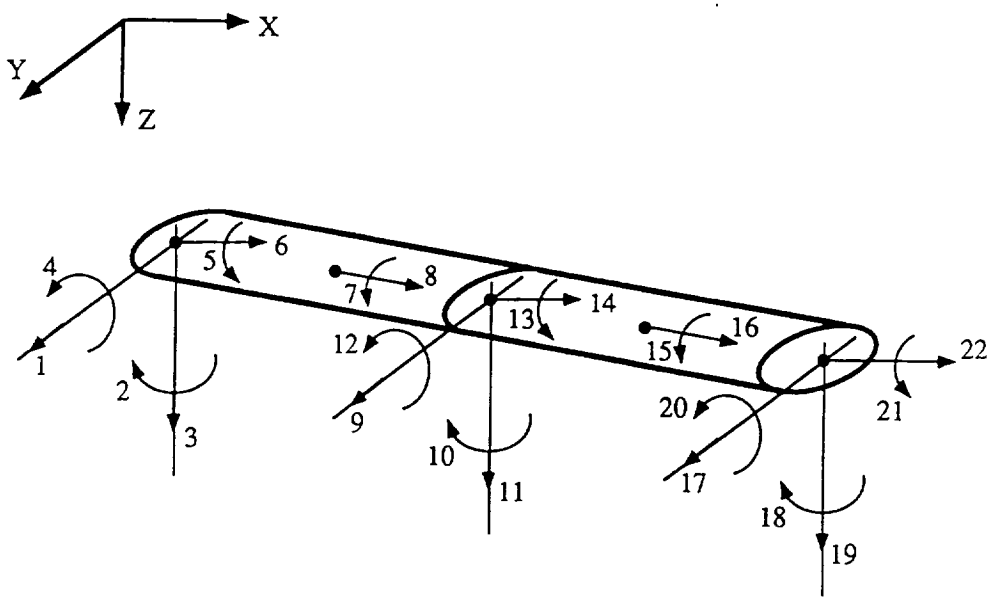

Figure 3-2. Definition of finite element degrees of freedom and schematic of the element ordering scheme.

rotation about the local z-axis and a small negative rotation about the local y-axis, respectively.

The transverse displacements, v and w, are interpolated using cubic Hermitian polynomials and quadratic polynomials are used to interpolate the torsional and axial deformations. This is the simplest element interpolation scheme yielding a consistent formulation for coupled torsion-bending (Ref. 23). Specifically:

$$
\begin{aligned}
v(x) &= \{\Phi_3\}^T \begin{Bmatrix} q_1 \\ q_2 \\ q_3 \\ q_4 \end{Bmatrix} \\
w(x) &= \{\Phi_3\}^T \begin{Bmatrix} q_5 \\ q_6 \\ q_7 \\ q_8 \end{Bmatrix} \\
\theta(x) &= \{\Phi_2\}^T \begin{Bmatrix} q_9 \\ q_{10} \\ q_{11} \end{Bmatrix} \\
u(x) &= \{\Phi_2\}^T \begin{Bmatrix} q_{12} \\ q_{13} \\ q_{14} \end{Bmatrix}
\end{aligned}
\tag{3.3}
$$

where,

$$
\{\Phi_3\} = \begin{Bmatrix} 1 - 3\xi^2 + 2\xi^3 \\ (\xi - 2\xi^2 + \xi^3)\,\ell \\ 3\xi^2 - 2\xi^3 \\ (-\xi^2 + \xi^3)\,\ell \end{Bmatrix} ; \quad \{\Phi_2\} = \begin{Bmatrix} 1 - 3\xi + 2\xi^2 \\ 4\xi - 4\xi^2 \\ -\xi + 2\xi^2 \end{Bmatrix}
\tag{3.4}
$$

and $\xi = x/\ell$. The preceding relations may be expressed in compact form as:

$$
\begin{Bmatrix} v(x) \\ w(x) \\ \theta(x) \\ u(x) \end{Bmatrix} = [\,\Phi\,]\,\{q\}
\tag{3.5}
$$

where $\{q\}$ is the vector of generalized displacements and $[\,\Phi\,]$ is a (4 x 14) matrix appropriately constructed from Equations 3.3 and 3.4.

The global degrees of freedom are obtained by resolving the deformations along the global axes using the transformation matrix derived previously. At an end node, all of the three translational and three rotational d.o.f. are available (since the slopes of the transverse bending displacements correspond to rotations). Thus, the translation between the local

element d.o.f.'s, $\{q\}_L$, and the global ones, $\{q\}_G$, is achieved using a straightforward transformation involving the matrix, T_{rot} :

$$\begin{Bmatrix} U \\ V \\ W \end{Bmatrix} = [T_{rot}] \begin{Bmatrix} u \\ v \\ w \end{Bmatrix} \; ; \qquad \begin{Bmatrix} R_X \\ R_Y \\ R_Z \end{Bmatrix} = [T_{rot}] \begin{Bmatrix} \theta \\ -w_{,x} \\ v_{,x} \end{Bmatrix} \tag{3.6}$$

where R_X, R_Y, and R_Z, are rotations due to deformation about the global XYZ axes respectively. At the mid-node the global deformations are *defined* to coincide with the respective local ones, i.e.,

$$\begin{Bmatrix} q10 \\ q13 \end{Bmatrix}_G = \begin{Bmatrix} q10 \\ q13 \end{Bmatrix}_L \tag{3.7}$$

This both simplifies the transformation and results in an orthogonal element transformation matrix, i.e., if the elemental transformation which will be composed of elements of $[T_{rot}]$ is denoted by $[T_{GL}]$ so that $\{q\}_G = [T_{GL}]\{q\}_L$ then $[T_{GL}]^{-1} = [T_{GL}]^T$.

3.1.3 Derivation of the Element Strains and Stresses

In order to compute the elemental stiffness matrix the strains arising from the preceding displacements must be evaluated. The nonlinear expressions for the strains are stated:

$$\begin{aligned} \varepsilon_{xx} &= u_{,x} + (\Psi\theta_{,x})_{,x} + \frac{1}{2}(\eta^2 + \zeta^2)\,\theta_{,x}^2 \\ &+ \frac{1}{2} v_{,x}^2 - v_{,xx}\{\eta\cos(\beta+\theta) - \zeta\sin(\beta+\theta)\} \\ &+ \frac{1}{2} w_{,x}^2 - w_{,xx}\{\zeta\cos(\beta+\theta) + \eta\sin(\beta+\theta)\} \end{aligned} \tag{3.8a}$$

$$\gamma_{x\eta} = 2\varepsilon_{x\eta} = (\Psi_{,\eta} - \zeta)(\theta_{,x} + \theta_{nl}) \tag{3.8b}$$

$$\gamma_{x\zeta} = 2\varepsilon_{x\zeta} = (\Psi_{,\zeta} + \eta)(\theta_{,x} + \theta_{nl}) \tag{3.8c}$$

and all other strains are assumed zero. Here, η and ζ, are the principal axes of the cross-section which are oriented such that:

$$\int_A \eta\zeta \, dA = 0 \tag{3.9}$$

In RotorCRAFT, the angle β between the local y and η axes is specified by the user in the cross-section input file. In Equations 3.8, θ_{nl} is a nonlinear 2^{nd} order torsion term,

and $\Psi(x,\eta,\zeta)$ is the Saint Venant warping function expressing the out-of-plane displacement, u_{warp} , due to torsion:

$$u_{warp}(x,\eta,\zeta) = \Psi(x,\eta,\zeta)\,\theta_{,x} \tag{3.10}$$

The linear expressions are easily obtained from above:

$$\begin{aligned}\varepsilon_{xx} &= u_{,x} + (\Psi\theta_{,x})_{,x} \\ &\quad - v_{,xx}\{\eta\cos\beta - \zeta\sin\beta\} - w_{,xx}\{\zeta\cos\beta + \eta\sin\beta\}\end{aligned} \tag{3.11a}$$

$$\gamma_{x\eta} = (\Psi_{,\eta} - \zeta)\,\theta_{,x} \;;\; \gamma_{x\zeta} = (\Psi_{,\zeta} + \eta)\,\theta_{,x} \tag{3.11b,c}$$

These strains are expressed in terms of the vector of generalized d.o.f., $\{q\}$, and the shape functions and their derivatives w.r.t. x , by substituting for the occurrences of u , v , w , and θ using Equations 3.3-3.5. This results in:

$$\varepsilon_{xx} = \begin{Bmatrix} -[\eta\cos\beta - \zeta\sin\beta]\{\Phi_3''\} \\ -[\zeta\cos\beta + \eta\sin\beta]\{\Phi_3''\} \\ \Psi_{,x}\{\Phi_2'\} + \Psi\{\Phi_2''\} \\ \{\Phi_2'\} \end{Bmatrix}^T \{q\} \tag{3.12a}$$

$$\begin{Bmatrix} \gamma_{x\eta} \\ \gamma_{x\zeta} \end{Bmatrix} = \begin{Bmatrix} \Psi_{,\eta} - \zeta \\ \Psi_{,\zeta} + \eta \end{Bmatrix} \begin{Bmatrix} 0 \\ 0 \\ \{\Phi_2'\} \\ 0 \end{Bmatrix}^T \{q\} \tag{3.12b}$$

The corresponding stresses are derived from the Hooke's Law:

$$\sigma_{xx} = E\,\varepsilon_{xx} \tag{3.13a}$$

$$\sigma_{x\eta} = G\,\gamma_{x\eta} \;;\; \sigma_{x\zeta} = G\,\gamma_{x\zeta} \tag{3.13b,c}$$

These expressions are used both in the construction of the stiffness matrices and in the evaluation of the stresses at specified locations on the blade. The former involves integrated quantities of the shape functions and cross-section and material properties, whereas the latter requires knowledge of the local coordinates where the stress is to be evaluated and warping function related quantities evaluated at the required x-location.

3.2 Evaluation of the Stiffness and Mass Matrices

The discussion above defines the relationships for stresses and strains for the current F.E. formulation. Reference 2 describes the procedure for obtaining the element stiffness and mass matrices via application of the Extended Hamilton's Principle, and the assembly of the corresponding global matrices. Briefly, the process begins by deriving expressions

for the kinetic and strain energies of each element. Any remaining forces not accounted for in the kinetic and strain energy expression, in particular the forces and geometric stiffening due to blade rotation, are represented by an external virtual work term. Variational calculus is then applied to the Lagrangian, $\mathcal{L}$ = (Kinetic Energy) -(Strain Energy), which yields the equations of motion that govern the blade dynamics. Since in this case the variation of the strain energy is equivalent to the internal virtual work which can be written down directly,

$$W^i = \int_V \sigma_{xx} \cdot \delta\varepsilon_{xx} + \sigma_{x\eta} \cdot \delta\gamma_{x\eta} + \sigma_{x\xi} \cdot \delta\gamma_{x\xi} \; dV \qquad (3.14)$$

the preliminary step of obtaining an expression for the strain energy is circumvented. The mass matrix is derived from those components of the kinetic energy expression containing products of the deformation velocities. The stiffness matrix is more complicated containing contributions from the strain energy, kinetic energy and from the external virtual work term representing the geometric stiffening. The volume integral is conveniently represented by an integral over the blade cross-section area, followed by an integral along the element length. Performing the area integration produces cross-section parameters such as area, first and second moments of area, torsion constant, etc., which in RotorCRAFT are supplied by the user in the blade cross-section input file. The integration along the element length is accomplished by 4 point Gaussian quadrature.

3.2.1 Assembly of the Global Mass and Stiffness Matrices

The element matrices obtained above are assembled into corresponding global matrices for the complete helicopter blade. The assembly process involves two sub-procedures: the first involves referring the elemental matrices and nodal forces to the global axes, and the second defines the array indexing that relates the local degrees of freedom for each element to the global ones.

Rotation of the element matrices and nodal forces into a global coordinate frame is accomplished in the standard manner:

$$\begin{aligned} [K_{global}] &= [T_{GL}]\,[K_{local}]\,[T_{GL}]^T \\ [M_{global}] &= [T_{GL}]\,[M_{local}]\,[T_{GL}]^T \\ \{F\}_{global} &= [T_{GL}]\,\{F\}_{local} \end{aligned} \qquad (3.15)$$

as may be easily verified by noting that the kinetic and potential energies and the virtual work are independent of the choice of reference frame. Here, $[T_{GL}]$ is the transformation matrix described in Section 3.1 relating local and global generalized d.o.f.: $\{q_{global}\} = [T_{GL}]\{q_{local}\}$.

The blade elements are then laid end to end in sequence from blade root to blade tip. Global deformations are defined as outlined in Equation 3.6. However, the ordering of the global degrees of freedom is different from the local ones. Each element degree of freedom is associated with a global one via an indexing array or splay matrix, C(k,ie) , where k is the local degree of freedom (k=1,2,...14) , ie is the element number, and C(k,ie) is the global degree of freedom. Having specified a C(k,ie) for each element then the global matrices may be constructed by 'splaying' components of the elemental mass and stiffness matrices into their corresponding positions in the global matrices. For example, the [i,j] entry of the elemental stiffness matrix for finite element, ie, is added to the

[C(i,ie),C(j,ie)] entry of the global stiffness matrix. In like manner, the global nodal force vector is built up from nodal forces for each element. Section 5 of Reference 2 details the definitions of the local and global degrees of freedom.

To this point in the development, the boundary conditions at the root have not been imposed, and some of the root degrees of freedom are eliminated when these are applied. For articulated blades, it is implicitly assumed in RotorCRAFT that the blade is freely hinged in both flap and lag directions, but that the remaining degrees of freedom at the root - the three translational displacements and the twist about the X axis - are constrained. Thus, the rows and columns of the global mass and stiffness matrices corresponding to these four degrees of freedom are removed prior to conducting the modal analysis. For cantilevered blades, by definition all root deformations are zero and thus all six degrees of freedom at the root are similarly eliminated. However, although the rows and columns corresponding to the constrained degrees of freedom are removed when computing the natural blade modes, they are employed when determining the inertia forces due to cyclic pitching, and also when calculating hub loads.

Let the global mass and stiffness matrices for the blade be given by:

$$M = \begin{bmatrix} M_{cc} & : & M_{cr} \\ \cdots & \cdots & \cdots \\ M_{rc} & : & M_{rr} \end{bmatrix} \quad ; \quad K = \begin{bmatrix} K_{cc} & : & K_{cr} \\ \cdots & \cdots & \cdots \\ K_{rc} & : & K_{rr} \end{bmatrix} \tag{3.16}$$

where the matrices have been partitioned into submatrices associated with constrained and unconstrained nodal degrees of freedom respectively. Submatrices, $[M_{rr}]$ and $[K_{rr}]$ are the mass and stiffness matrices for unconstrained deformations and are used in computing modal properties. The constrained degrees of freedom are associated with the translational deformations, U, V , and W, and also the twist rotation, R_X, at the blade root. For cantilevered beams, the constrained degrees of freedom also include the rotations, R_Y and R_Z. Of particular interest are the matrix partitions associated with the root twist displacement, θ_c , which shall be required for computing the effects of cyclic pitch. Although the twist deformation is zero at the root, it is clear that there is a finite rigid body rotation occurring at the root due to cyclic pitching and this will introduce an associated inertia term into the equations of motion governing the remaining degrees of freedom. The equations of motion obtained from the Extended Hamilton's Principle are summarized here (see Ref. 2 for details) as:

$$[\, M_{r\theta_c} : M_{rr} \,] \begin{Bmatrix} \ddot{\theta}_c \\ \cdots \\ \ddot{q}_r \end{Bmatrix} + [\, K_{r\theta_c} : K_{rr} \,] \begin{Bmatrix} \theta_c \\ \cdots \\ q_r \end{Bmatrix} = \{F^{aero}\} + \{F^{rot}\} \tag{3.17}$$

where $[M_{r\theta_c}]$ and $[K_{r\theta_c}]$ are the column of the mass and stiffness matrices associated with the root twist, $\{F^{aero}\}$ are the nodal forces due to aerodynamic loads and $\{F^{rot}\}$ the nodal forces associated with the blade rotation. This last term is time invariant and therefore need only be computed once for a given blade rotation speed. Note that none of the other

constrained degrees of freedom, U, V, W, (and R_y , R_z , for cantilevered blades) are zero and so do not appear in Equation 3.17. The only non-zero root displacement is θ_c.

The generalized displacement vector, $\{q_r\}$, includes both deformation effects and the rigid body rotation due to cyclic pitch. It is convenient to define deformation variables $\{q\}$ by subtracting the rigid body motion arising from cyclic pitch. These represent deformations relative to a set of axes rotating with the blade root.

$$\{q\} = \{q_r\} - \{r_{\theta_c}\}\theta_c \quad ; \quad \{\ddot{q}\} = \{\ddot{q}_r\} - \{r_{\theta_c}\}\ddot{\theta}_c \tag{3.18}$$

where $\{r_{\theta_c}\}$ is the vector of generalized displacements arising from unit root pitch. The components of $\{r_{\theta_c}\}$ may be computed explicitly from the geometry as the global displacements and rotations due to unit cyclic pitch:

$$\begin{aligned} &U = 0 \; ; \quad V = -r_Z \quad ; \quad W = r_Y \\ &\theta_X = 1 \; ; \quad R_Y = 0 \quad ; \quad R_Z = 0 \end{aligned} \tag{3.19}$$

Here r_Y and r_Z are the global Y and Z coordinates of the elastic axis at a given location along the blade. One can also compute $\{r_{\theta_c}\}$ from

$$\{r_{\theta_c}\} = - [K_{rr}]^{-1} [K_{r\theta_c}] \tag{3.20}$$

which is obtained simply by noting that rigid body rotations do not contribute to material strains. Strictly speaking, the latter expression is an approximation valid for small pitch angles. The effects of geometric stiffening are in fact dependent upon the orientation of the structure. Thus, changing θ_c alters the geometric stiffening entries of $[K_{rr}]$. Large cyclic inputs imply that the rotating frame acquires significant angular velocity and acceleration components along the global X-axis in addition to the steady angular velocity arising from blade rotation. A full analysis accounting for the various cross-products of translational and angular velocities would be necessary, as is done say, in slewing manoeuvres of spinning satellites. In the present case, such an analysis is unwarranted in light of the linearization assumptions already made in the F.E. analysis and the small cyclic pitch amplitudes under consideration here.

Rearranging Equation 3.17:

$$[M_{rr}]\{\ddot{q}_r\} + [K_{rr}]\{q_r\} = \{F^{aero}\} + \{F^{rot}\} - \left([M_{r\theta_c}]\ddot{\theta}_c + [K_{r\theta_c}]\theta_c \right) \tag{3.21}$$

and distinguishing between the blade deformations and rigid body displacements via Equation 3.18

$$\begin{aligned} [M_{rr}]\{\ddot{q}\} + [K_{rr}]\{q\} &= \{F^{aero}\} + \{F^{rot}\} - \left([M_{r\theta_c}]+[M_{rr}]\{r_{\theta_c}\} \right)\ddot{\theta}_c \\ &\quad - \left([K_{r\theta_c}]+[K_{rr}]\{r_{\theta_c}\} \right)\theta_c \\ &= \{F^{aero}\} + \{F^{rot}\} - \left([M_{r\theta_c}] + [M_{rr}]\{r_{\theta_c}\} \right)\ddot{\theta}_c \end{aligned} \tag{3.22}$$

where use is made of Equation 3.20 in the final equality.

3.2.2 Computation of Modal Properties

The dynamic analysis in the RotorCRAFT code is formulated in terms of the response modes of the blade. Thus, the information contained in the blade mass and stiffness matrices is used to obtain a set of mode shapes and their corresponding modal frequencies and masses. The modes are obtained by solving the generalized eigenvalue problem:

$$[K_{rr}]\{x_i\} = \omega_i^2[M_{rr}]\{x_i\} \tag{3.23}$$

where ω_i is the natural frequency of the i-th mode, and $\{x_i\}$ is the corresponding eigenvector, or, mode shape.

Equation 3.23 is solved using the an efficient and accurate generalized Jacobi iteration method described in Reference 24. The modes are then ordered in ascending frequency, and sorted into the dominant type of deformation present in each mode: bending (flap and lag), torsion or extension. The number of modes of each type retained in the dynamic analysis in RotorCRAFT is specified by the user.

Having obtained a set of modal frequencies and shapes, the generalized deformation, $\{q\}$, may be expressed in terms of modal amplitudes, $\{\eta\}$, as:

$$\{q\} = [X]\{\eta\} \tag{3.24}$$

where $[X] = [\ \{x_i\}\ ]$ is the set of column eigenvectors of the retained modes. Equation 3.22 may then be transformed into the modal variables by pre-multiplying by $[X]^T$ and substituting $\{q\}=[X]\{\eta\}$:

$$[X]^T[\,M_{rr}\,][X]\{\ddot{\eta}\} + [X]^T[\,K_{rr}\,][X]\{\eta\}$$
$$= \quad [X]^T\left[\,\{F^{aero}\} + \{F^{rot}\} - \left([M_{r\theta_c}] + [M_{rr}]\{r_{\theta_c}\}\right)\ddot{\theta}_c\,\right]$$

or, $$GM(i)\left[\,\ddot{\eta}_i + \omega_i^2\,\eta_i\,\right] = F^{AERO}(i) + F^{ROT}(i) - MRC(i)\,\ddot{\theta}_c \tag{3.25}$$

where,

$$GM(i) = \{x_i\}^T[\,M_{rr}\,]\{x_i\} \tag{3.26a}$$

$$\omega_i^2 = \frac{1}{GM(i)}\ \{x_i\}^T[\,K_{rr}\,]\{x_i\} \tag{3.26b}$$

$$F^{AERO}(i) = \{x_i\}^T\ \{F^{aero}\} \tag{3.26c}$$

$$F^{ROT}(i) = \{x_i\}^T\ \{F^{rot}\} \tag{3.26d}$$

and, $$MRC(i) = \{x_i\}^T\left([M_{r\theta_c}] + [M_{rr}]\{r_{\theta_c}\}\right) \tag{3.26e}$$

The generalized mass, GM(i), is determined by the normalization method of $\{x_i\}$. In RotorCRAFT, the modeshapes are normalized so as to have tip amplitude equal to the blade radius. Thus, for the first flap and lag modes, GM(i) is approximately the second moment of inertia of the blade about the hinge and the modal amplitudes, $\{\eta\}$, correspond to flap and lag angles.

3.3 Computation of Loads and Blade Stresses

3.3.1 Hub Loads

Hub loads are computed from the equations of motion corresponding to the constrained nodes:

$$\{F_c\} = [M_{c\theta_c} : M_{cr}] \begin{Bmatrix} \ddot{\theta}_c \\ \cdots \\ \ddot{q}_r \end{Bmatrix} + [K_{c\theta_c} : K_{cr}] \begin{Bmatrix} \theta_c \\ \cdots \\ q_r \end{Bmatrix} \tag{3.27}$$

where $[M_{c\theta_c}]$ and $[K_{c\theta_c}]$ are the column vectors of $[M_{cc}]$ and $[K_{cc}]$ respectively corresponding to the root twist deformation. The terms: $[K_{cr}]$, $[M_{cr}]$, $[M_{c\theta_c}]$, and $[K_{c\theta_c}]$ are directly extracted from the assembled finite element matrices prior to the constraint deletion procedure. The constraint forces, $\{F_c\}$, are interpreted as the forces that must be imposed upon the blade in order to effect the constraint conditions. Therefore, the equal and opposite hub forces (experienced by the hub) are $\{F^{hub}\} = -\{F_c\}$. If $q_r(t)$ is known, then one can in principle compute the constraint forces at the blade root. From the same arguments following Equation 3.20, one may rewrite the last term involving the stiffness matrix to obtain:

$$\{F_c\} = [M_{c\theta_c} : M_{cr}] \begin{Bmatrix} \ddot{\theta}_c \\ \cdots \\ \ddot{q}_r \end{Bmatrix} + [K_{cr}]\{q\} \tag{3.28}$$

with $\{q\}$ defined in Equation 3.18.

Potential difficulties in the computation of hub loads may arise when higher modes modes are neglected and $q_r(t)$ is constructed from a reduced set of modal responses. Neglected modes which are unimportant when predicting aerodynamic loads and blade deflections may be quite significant in hub force computation. Consider for example the extension response of the blade. In most rotor blades, the frequency of extensional vibration is an order of magnitude greater than the torsional, flap and lag frequencies. Furthermore, the aerodynamic force component along the blade is usually negligible and the contribution of the blade stretching dynamics to the overall motion can thus be ignored. However, the forces due to blade rotation act primarily in the direction along the blade and thus the chief hub load arising from blade rotation acts in the X-direction which is precisely the axis along which the extensional motion occurs. So if extension modes are neglected in the analysis and hub forces are computed from $\{q\}=[X]\{\eta\}$ and Equation 3.28 then the dominant hub force in the X-direction due to blade rotation will be completely neglected. The fundamental issue is that the contributing forces may have significant components that are orthogonal to the space spanned by the retained modal set.

To remedy this situation, it has been found useful to compute certain of the hub force contributions directly, and to then superimpose the effects due to the modal accelerations. The simplest derivation is to suppose one has retained all of the modes in the analysis so that the original F.E. model and the modal analysis yield identical results, to then evaluate all those forcing terms that can be computed directly, and to finally approximate the remaining terms with a restricted mode set.

Rewriting Equation 3.28

$$\{F_c\} = [M_{c\theta_c}]\ddot{\theta}_c + [M_{cr}]\{\ddot{q}_r\} + [K_{cr}]\{q\} \tag{3.29}$$

and substituting for $\{q\}$ and $\{\ddot{q}_r\}$ using Equations 3.18 and 3.24,

$$\{F_c\} = [M_{cr}][X]\{\ddot{\eta}\} + \left([M_{c\theta_c}] + [M_{cr}]\{r_{\theta_c}\} \right)\ddot{\theta}_c + [K_{cr}][X]\{\eta\} \tag{3.30}$$

where $\{r_{\theta_c}\}$ is computed from Equation 3.20 and [X] follows from the eigenanalysis, Equation 3.23. Using the modal equations, Equation 3.25, to solve for $\{\eta\}$:

$$\{\eta\} = [D]^{-1}\left[\{F^{AERO}\} + \{F^{ROT}\} - \{MRC\}\ddot{\theta}_c\right] - [\,\mathrm{diag}\{\,1/\omega_i^2\,\}]\{\ddot{\eta}\} \tag{3.31}$$

where $[D] = [\,\mathrm{diag}\{\,\omega_i^2\,GM(i)\,\}\,]$. Substituting for $\{\eta\}$ in Equation 3.30 using Equation 3.31 and collecting terms:

$$\begin{aligned}\{F_c\} &= \left([M_{cr}][X] - [K_{cr}][X][\,\mathrm{diag}\{\,1/\omega_i^2\,\}]\right)\{\ddot{\eta}\} \\ &\quad + \left([M_{c\theta_c}] + [M_{cr}]\{r_{\theta_c}\} - [K_{cr}][X][D]^{-1}\{MRC\}\right)\ddot{\theta}_c \\ &\quad + [K_{cr}][X][D]^{-1}\left[\{F^{AERO}\} + \{F^{ROT}\}\right]\end{aligned} \tag{3.32}$$

The last two terms:

$$[K_{cr}][X][D]^{-1}\left[F^{AERO}(i) + F^{ROT}(i)\right] = [K_{cr}][X][D]^{-1}[X]^T\left[\{F^{aero}\} + \{F^{rot}\}\right]$$

but since

$$[X][D]^{-1}[X]^T = [X]([X]^T[K_{rr}][X])^{-1}[X]^T = [K_{rr}]^{-1} \tag{3.33}$$

Equation 3.32 becomes,

$$\begin{aligned}\{F_c\} &= \left([M_{cr}][X] - [K_{cr}][X][\,\mathrm{diag}\{\,1/\omega_i^2\,\}]\right)\{\ddot{\eta}\} \\ &\quad + \left([M_{c\theta_c}] + [M_{cr}]\{r_{\theta_c}\} - [K_{cr}][X][D]^{-1}\{MRC\}\right)\ddot{\theta}_c \\ &\quad + [K_{cr}][K_{rr}]^{-1}\left[\{F^{aero}\} + \{F^{rot}\}\right]\end{aligned}$$

$$= [MFC]\{\ddot{\eta}\} + \{MCYC\}\ddot{\theta}_c + \{F^{AEROC}\} + \{F^{ROTC}\} \tag{3.34}$$

where

$$[MFC] = [M_{cr}][X] - [K_{cr}][X][\,diag\{\,1/\omega_i^2\,\}] \tag{3.35a}$$

$$\{MCYC\} = [M_{c\theta_c}] + [M_{cr}]\{r_{\theta_c}\} - [K_{cr}][X][D]^{-1}\{MRC\} \tag{3.35b}$$

$$\{F^{AEROC}\} = [K_{cr}][K_{rr}]^{-1}\{F^{aero}\} \tag{3.35c}$$

$$\{F^{ROTC}\} = [K_{cr}][K_{rr}]^{-1}\{F^{rot}\} \tag{3.35d}$$

and {MRC} is the vector with components defined in Equation 3.26e.

Fortunately, the forces due to steady blade rotation are constant, and thus $\{F^{ROTC}\}$ is constant and need only be computed once. Furthermore, it does not contribute to the modal accelerations but in effect induces a steady state bias in the $\{\eta\}$. This implies that no error in the rotational force contribution to the hub forces is incurred when using a reduced set of modes since the remaining quantities in Equation 3.34, $\{\ddot{\eta}\}$, $\ddot{\theta}_c$ and $\{F^{aero}\}$ are independent of the rotational force. In other words, all of the rotation force contribution is contained in $\{F^{ROTC}\}$.

The term,

$$[K_{cr}][K_{rr}]^{-1} = ([K_{rr}]^{-1}[K_{rc}])^T \tag{3.36}$$

can be shown to be the transpose of the array whose k-th row corresponds to a unit displacement in the negative k-th Cartesian direction. For example, if the beam were given a unit displacement in the negative Y direction (corresponding to k=2) then the resulting vector $\{q\} = ([K_{rr}]^{-1}[K_{rc}])_{k=2}$. This is completely analogous to the definition of $\{r_{\theta_c}\}$ in Equation 3.20. Here, Cartesian directions, k=1,2,3 correspond to displacements along the rotating blade X,Y,Z axes respectively, and k=4,5,6 correspond to rotations about those axes. Therefore, $\{F^{AEROC}\}$ is simply the summation of the aerodynamic nodal forces in the k-th Cartesian direction which is obtained in RotorCRAFT by summing the aerodynamic forces and moments about the hinge directly. So,

$$\{F^{AEROC}\} = \int_{cutout}^{tip} \{F\}^{aero}\, ds = \begin{Bmatrix} F_X^{aero} \\ Drag \\ -Thrust \\ M_X^{aero} \\ \cdots \\ M_Y^{aero} \\ M_Z^{aero} \end{Bmatrix} \tag{3.37}$$

which is equivalent to the aerodynamic force and moment vectors defined in Equations 2.11 and 2.12 when referred to the rotating blade axes. Equation 3.34 is used in the same form when a reduced set of modes is employed. {MCYC} is evaluated in terms of the reduced mode set rather than the complete set since the cyclic pitch acceleration influences the modal accelerations so that the combination of the terms involving $\{\ddot{\eta}\}$ and $\ddot{\theta}_c$ in Equation 3.34 is consistent. Computing the aerodynamic loading via Equation 3.37 rather than in terms of the reduced modes is consistent since the error incurred is of the same order as that due to neglecting higher modes in the first place. Furthermore, the hub loads averaged over one blade rotation equal the correspondingly averaged aerodynamic forces, as is expected theoretically. This is not generally true if the hub loads are computed based on the reduced set of aerodynamic modal forces, $\{F^{AERO}\}$. The computed hub loads are seen to correspond to a blade subject to the true aerodynamic loads but with the accelerations determined from the restricted set of modes.

3.3.2 Blade Stress Calculations

The linearized longitudinal and cross-section shear stresses follow directly from Equations 3.12 and 3.13:

$$\sigma_{xx} = E \begin{Bmatrix} -[\eta\cos\beta - \zeta\sin\beta]\{\Phi_3''\} \\ -[\zeta\cos\beta + \eta\sin\beta]\{\Phi_3''\} \\ \Psi_{,x}\{\Phi_2'\} + \Psi\{\Phi_2''\} \\ \{\Phi_2'\} \end{Bmatrix}^T \{q\}_L \tag{3.38}$$

$$\begin{Bmatrix} \sigma_{x\eta} \\ \sigma_{x\zeta} \end{Bmatrix} = G \begin{Bmatrix} \Psi_{,\eta} - \zeta \\ \Psi_{,\zeta} + \eta \end{Bmatrix} \begin{Bmatrix} 0 \\ 0 \\ \{\Phi_2'\} \\ 0 \end{Bmatrix}^T \{q\}_L \tag{3.39}$$

where the subscript, L, denotes local generalized coordinates. Both the longitudinal and shear stresses are functions of the area coordinates, η and ζ, which must be specified. Furthermore, the stresses are most conveniently referred to the local reference frame which is desirable since the remaining components of the stress tensor are zero by assumption. Referring stresses to the global blade fixed axes, though straightforward in principle, results in an awkward description of the stress distribution where, in general, all six of the stress components are non-zero.

Note that while this treatment is adequate for straight, uniform blades, inconsistencies in the stresses referred to the local element axes arise when there is a discontinuity in sweep, anhedral or other structural or geometrical property between elements. i.e., a plot of, say, σ_{xx} as function of x for a general blade topology will exhibit discontinuities. In theory, near such points, the stress tensor is full and the simplified beam theory is not valid. However, by assumption, the changes in sweep, anhedral, etc., between elements are gradual (see the discussion in Sect. 5 of Ref. 2) and the error introduced by a suitable stress averaging procedure should be small. In addition, St. Venant's Principle is applicable to the model so that stress and strain states are only strictly valid in regions away from the blade ends and points where discontinuities in the blade geometry or structural properties occur.

The stress at such points may be approximated by either: 1) referring the stress of each element to an 'average reference frame' and averaging these resulting stresses, or 2) merely averaging the stresses of each element. An average reference frame is here defined in terms of the anhedral and sweep that are averaged from the two adjacent elements. Presently, no averaging is done and the code simply chooses one of the elements and refers stresses in the local coordinates of that element.

The nodal deformations are determined from the modal amplitudes and any remaining steady state contributions from the blade rotation forces. Note that the actual displacement of each node also includes the rigid blade motion due to the cyclic pitch. However, this component of the motion does not contribute to the stresses since no deformations are associated with rigid body movement. Thus, from the original expression for the nodal displacements (in global coordinates), Equation 3.18:

$$\{q_r\} = [X]\{\eta\} + \{r_{\theta c}\}\theta_c + \{\tilde{q}^{rot}\} \tag{3.40}$$

where $\{r_{\theta c}\}$ is the nodal displacement vector due to unit cyclic pitch and the residual:

$$\{\tilde{q}^{rot}\} = \left([K_{rr}]^{-1} - [X][D]^{-1}[X]^T \right) \{F^{rot}\} \tag{3.41}$$

where, $[D] = [\ \text{diag}\{\ \omega_i^2\, GM(i)\ \}\ ]$ is added to compensate for neglected modes in the analysis. This follows from the steady state deflection due to blade rotation obtained from the complete finite element analysis,

$$\{q^{rot}\} = [K_{rr}]^{-1}\{F^{rot}\} \tag{3.42}$$

and the steady state deflection obtained by modal reconstruction,

$$\begin{aligned} \{q^{rot}\} &= \sum_{i=1}^{NMODE} \{x(i)\} \frac{1}{\omega_i^2\, GM(i)} F^{ROT}(i) \\ &= [X]\left[\text{diag}\{ \frac{1}{\omega_i^2\, GM(i)} \}\right] [X]^T \{F^{rot}\} \end{aligned} \tag{3.43}$$

As noted previously, this correction is necessary when the set of retained modes does not include an extension mode and thus is orthogonal to the rotational force vector. Without this adjusting term, the deflections due to the substantial rotational force would be unaccounted for thus resulting in substantial hub forces and axial stress errors. The actual deformations from Equation 3.18 are

$$\begin{aligned} \{q\} &= \{q_r\} - \{r_c\}\theta_c \\ &= [X]\{\eta\} + \left([K_{rr}]^{-1} - [X][D]^{-1}[X]^T \right) \{F^{rot}\} \end{aligned} \tag{3.44}$$

These deformations are then referred to the local reference frames with Equations 3.38 and 3.39 being used to obtain the blade stresses.

Procedurally, this is most easily accomplished in parallel with the construction of the array, SHAPES(nm,ir,k) which is the modal deflection, k, of mode, nm, at radial location, ir. Considering first the longitudinal stress:

$$\sigma_{xx} = E \begin{Bmatrix} -[\eta\cos\beta - \zeta\sin\beta]\{\Phi_3''\} \\ -[\zeta\cos\beta + \eta\sin\beta]\{\Phi_3''\} \\ \Psi_{,x}\{\Phi_2'\} + \Psi\{\Phi_2''\} \\ \{\Phi_2'\} \end{Bmatrix}^T \left([X]\{\eta\} + \{\tilde{q}^{rot}\}\right) \quad (3.45)$$

The term in (•) is assumed to be referred to the local coordinate system of the element containing the point of interest. The full information necessary to determine σ_{xx} at any point on the cross-section is stored in the array SIGXX(nm,ir,k), where:

$$SIGXX(nm,ir,1) = -E\left\{\cos\beta\{\Phi_3''\}^T : \sin\beta\{\Phi_3''\}^T\right\}\begin{Bmatrix} x_1 \\ \vdots \\ x_8 \end{Bmatrix}_{nm}$$

$$SIGXX(nm,ir,2) = E\left\{\sin\beta\{\Phi_3''\}^T : -\cos\beta\{\Phi_3''\}^T\right\}\begin{Bmatrix} x_1 \\ \vdots \\ x_8 \end{Bmatrix}_{nm}$$

$$SIGXX(nm,ir,3) = E\{\Phi_2'\}^T\begin{Bmatrix} x_9 \\ x_{10} \\ x_{11} \end{Bmatrix}_{nm} \quad SIGXX(nm,ir,4) = E\{\Phi_2''\}^T\begin{Bmatrix} x_9 \\ x_{10} \\ x_{11} \end{Bmatrix}_{nm}$$

$$SIGXX(nm,ir,5) = E\{\Phi_2'\}^T\begin{Bmatrix} x_{12} \\ x_{13} \\ x_{14} \end{Bmatrix}_{nm} \quad (3.46)$$

where $\{x_1 \ldots x_{14}\}^T$ are the local coordinate deflections due to mode, nm. In particular, if the global deflections corresponding to mode, nm, for element, ie, are, $\{X_1 \ldots X_{14}\}^T$ (these are simply those D.O.F. of the modal vector, $\{X\}$, that correspond to element, ie) then, $\{x_1 \ldots x_{14}\}^T = [T_{rot}]^T\{X_1 \ldots X_{14}\}^T$. Then at any cross-section point, (η,ζ), at radial location, ir, the longitudinal stress generated by mode, nm, is

$$\begin{aligned} \sigma_{xx}(nm) = {} & \eta\, SIGXX(nm,ir,1) + \zeta\, SIGXX(nm,ir,2) \\ & + \Psi_{,x}\, SIGXX(nm,ir,3) + \Psi\, SIGXX(nm,ir,4) \\ & + SIGXX(nm,ir,5) \end{aligned} \quad (3.47)$$

and the total stress,

$$\sigma_{xx} = \sigma_{xx}(0) + \sum_{nm=1}^{NMODE} \sigma_{xx}(nm) \quad (3.48)$$

where the constant stress:

$$\begin{aligned} \sigma_{xx}(0) = {} & \eta\, SIGXX(0,ir,1) + \zeta\, SIGXX(0,ir,2) \\ & + \Psi_{,x}\, SIGXX(0,ir,3) + \Psi\, SIGXX(0,ir,4) \\ & + SIGXX(0,ir,5) \end{aligned} \quad (3.49)$$

and,

$$SIGXX(0,ir,1) = -E\left\{\cos\beta\,\{\Phi_3''\}^T \;:\; \sin\beta\,\{\Phi_3''\}^T\right\}\left\{\begin{array}{c}\tilde{q}_1^{tot}\\ :\\ \tilde{q}_8^{tot}\end{array}\right\}_L$$

$$SIGXX(0,ir,2) = E\left\{\sin\beta\,\{\Phi_3''\}^T \;:\; -\cos\beta\,\{\Phi_3''\}^T\right\}\left\{\begin{array}{c}\tilde{q}_1^{tot}\\ :\\ \tilde{q}_8^{tot}\end{array}\right\}_L$$

$$SIGXX(0,ir,3) = E\,\{\Phi_2'\}^T\left\{\begin{array}{c}\tilde{q}_9^{tot}\\ \tilde{q}_{10}^{tot}\\ \tilde{q}_{11}^{tot}\end{array}\right\}_L$$

$$SIGXX(0,ir,4) = E\,\{\Phi_2''\}^T\left\{\begin{array}{c}\tilde{q}_9^{tot}\\ \tilde{q}_{10}^{tot}\\ \tilde{q}_{11}^{tot}\end{array}\right\}_L$$

$$SIGXX(0,ir,5) = E\,\{\Phi_2'\}^T\left\{\begin{array}{c}\tilde{q}_{12}^{tot}\\ \tilde{q}_{13}^{tot}\\ \tilde{q}_{14}^{tot}\end{array}\right\}_L \qquad (3.50)$$

A similar procedure may be followed for the shear stresses, $\sigma_{x\eta}$ and $\sigma_{x\zeta}$. However, shear stresses are not currently implemented in RotorCRAFT.

In each case, the evaluation of the stress requires the specification of a particular point on the cross-section of the rotor blade. Typical strain gauge installations involve differencing the measured strain from different locations on the blade. Similarly, blade stress is most directly computed by evaluating the local stress at different locations on the blade and differencing the resulting predictions. Examples of such calculations are discussed in Section 5.

4. OVERVIEW OF CODE OPERATION

This section provides a brief summary of the trim procedures embedded in RotorCRAFT (Mod 1.0), with particular reference to the new provisions for arbitrary periodic pitch input. Also, the discussion below provides an outline of the preliminary interface developed here for interaction of RotorCRAFT with NASA's WOPWOP noise prediction code. It is emphasized at the outset that the present interface produces results that are considered suitable only for demonstration calculations and preliminary software development, not for correlation of acoustic data. The development of a more refined and complete analysis of rotor noise is the subject of ongoing research, the preliminary results of which are reported in References 25 and 26.

4.1 Rotor Trim Procedures in the Presence of Higher Harmonic Pitch

As discussed above and in Reference 2, the Mod 0.0 variant of the RotorCRAFT analysis was designed to solve for the aerodynamic loads on isolated helicopter rotors in steady forward flight. The rotor hub is assumed to be fixed in space and the rotor shaft is assumed to be oriented at a fixed angle with respect to the free stream. The solution method is directed at obtaining periodic solutions for the wake geometry, the blade motion, the aerodynamics loads, and now, in the Mod 1.0 variant, for the blade stresses and hub loading. This objective was judged to be appropriate for this particular effort, given the focus on steady-state forward flight. The "transient" solution achieved during the iteration process does not represent a time-accurate calculation of rotor loading; only the converged result can be considered physically valid and consistent. The approach used to obtain this converged result is now described.

The outermost loop in the iteration process is the computation of the evolution of the wake geometry over one rotor revolution with blade motion and aerodynamic loading fixed. The simulation is ordinarily run for a discrete number of rotor revolutions, and between each revolution the cyclic pitch inputs and the collective are adjusted to meet the conditions specified by the user for thrust and first harmonic flapping response (ordinarily, zero first harmonic flapping is desired, though many experimental cases in the literature have been run with nonzero flapping). This trim procedure represents the second loop within the overall iteration. Finally, the innermost loop is the calculation of the blade motion that is consistent with the current values of the pitch control settings; this calculation is carried out using the dynamic model described in Section 3 above and is performed assuming the wake-induced downwash is fixed at the most recent estimate obtained from the outer loop involving the wake evolution.

The principal change in this procedure in the Mod 1.0 variant is that the pitch command may now be of the form

$$\theta(\psi) = \theta_0 + \theta_{1c}\cos\psi + \theta_{1s}\sin\psi + \ldots + \theta_{nc}\cos n\psi + \theta_{ns}\sin n\psi + \ldots \qquad (4.1)$$

The root pitch may thus be adjusted to any desired set of harmonic inputs. In addition, the user may also select an arbitrary time history of root pitch inputs with the appropriate parameter selection, with the constraint that it be periodic with the rotor rotation. If the user wishes, the trim procedure can be switched off so that the cyclic pitch time history is fixed according to the specified parameters θ_{nc}, θ_{ns}. If not, the trim procedure will still leave the higher harmonic content of the cyclic pitch input unchanged, (θ_{nc} and θ_{ns} for $n > 1$), but will modify θ_{1c} and θ_{1s} until the user requested first harmonic rigid flapping values are obtained.

The first step in starting the overall solution procedure is to determine an initial estimate for the blade motion and the cyclic controls using the vortex lattice method and an estimate of wake-induced velocity based on a simple, prescribed downwash distribution. This calculation includes the higher harmonic pitch input, but can be bypassed in favor of an arbitrary periodic input, as noted above. Using the blade motion and bound circulation estimates so generated, the first loop of the analysis proceeds, beginning with a kinematic wake whose geometry is determined by the free stream and the downwash at the rotor disk. The wake then is allowed to evolve for one rotor revolution, during which the time history of the wake-induced flow field at each evaluation point on the rotor blade is computed and stored. At the end of this revolution, this time history of wake-induced flow is passed to a trim and dynamics routine that updates the control settings and the blade motion solution to be consistent with the free wake flow field.

If automatic trim has been selected, the program uses the updated velocity field and checks whether the first harmonic components of rigid flapping are within a specified tolerance of the desired level. If not, the cyclic pitch is adjusted and the blade motion calculation repeated until they are. Once trim has been achieved, the thrust is checked to see if it lies within a specified tolerance of the desired level. If not, the collective is adjusted and the steps just above are repeated until this condition is met. The iteration history for thrust coefficient is tracked and previous results are used to accelerate the convergence process. This process has proved to be sufficiently robust to handle a wide variety of rotor configurations, as will be evident from the sample cases presented in both Reference 2 and in Section 5 below. A flow chart of the sequence of events in the trim cycle is given in Figure 4-1; more information in the input requirements can be found in Reference 15, and a detailed discussion of the overall trim calculation can be found in Reference 2.

Once the blade motion solution has converged and the final aerodynamic loading distribution has been determined, the information needed for the computation of rotor blade hub loads and internal stresses is available. The computation of the hub loads proceeds as described in the previous section and produces time histories of the forces and moments exerted on the rotor hub, with the quantities expressed in the global (shaft) reference frame. The computation of the internal blade stress requires the specification of the radial and vertical positions of evaluation points relative to the blade's elastic axis (Ref. 15). The calculations described in Section 5 will include representative results of both stress and hub load computations.

4.2 WOPWOP Coupling

The development of comprehensive rotor noise prediction capabilities is a topic of ongoing research, and the development of efficient flow field prediction methods to support this work was the topic of recent NASA-sponsored research (Ref. 26). As a first step in adapting the flow field prediction code described in Reference 26 to the problem of noise prediction, a preliminary scheme has been developed for generating the unsteady blade surface pressure information required to carry out noise computations.

The primary objective of the present limited effort was to produce output from RotorCRAFT compatible with the input requirements of an independent acoustic program, WOPWOP, developed at NASA Langley (Ref. 27). WOPWOP was selected because of its robustness in analyzing general helicopter rotor configurations. The fundamentals of its acoustic analysis are based on Farassat's subsonic formulation of the Fowcs Williams-Hawkings equation derived for the noise generated by surfaces in arbitrary motion. Assuming that the surface loading distribution is known beforehand, Farassat's scheme

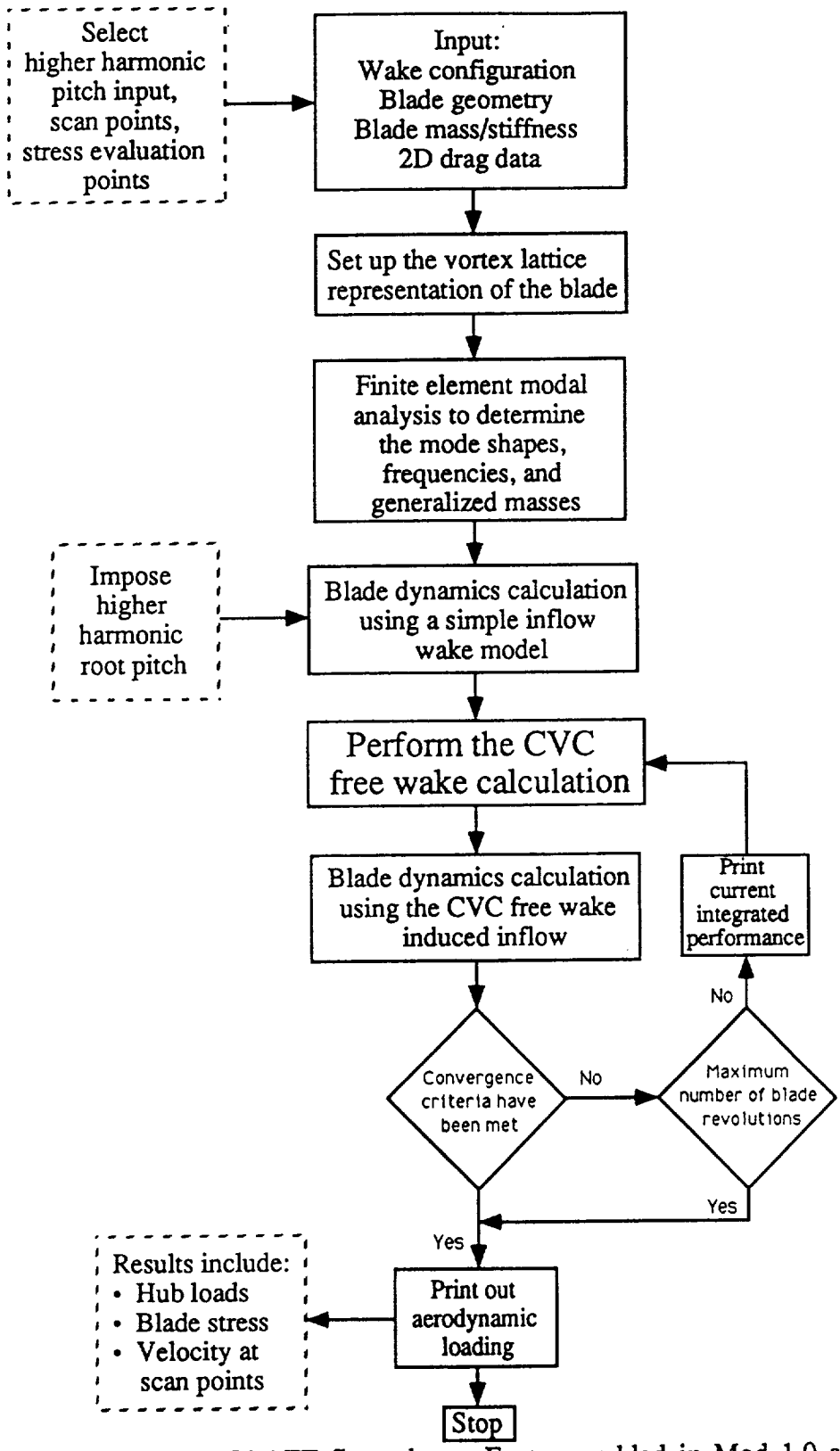

Figure 4-1. RotorCRAFT flow chart. Features added in Mod 1.0 are shown in dotted boxes.

provides an effective prediction of noise generated by surfaces in subsonic flow. The scheme implemented in WOPWOP was specially tailored for the helicopter rotor acoustic problem, and both the blade motions and surface pressures are required inputs to the program. The surface pressures, in particular, must be accurately specified to a high degree of resolution to obtain good noise predictions.

Since the Mod 0.0 version of RotorCRAFT focused largely on the prediction of aerodynamic loading that contributes to vibratory airloads, a substantial increase in refinement is required to determine a detailed distribution of chordwise airloads on the rotor blades. Substantial research work to date has been dedicated to develop practical models for the accurate solution of high-frequency surface airloads distribution for acoustics applications. Since many issues pertaining to the creation of a generally applicable model for unsteady loading remain unresolved, it was judged appropriate for current purposes to adopt a relatively simple model based on the selection of an aerodynamic transfer function to predict the lift response to the unsteady upwash field experienced by the rotor blades. The approach taken here is very similar to that described in Reference 26.

A routine designed to provide the necessary interface has been implemented in RotorCRAFT (Mod 1.0) as a post-processor to the rotor-wake calculation and is invoked only after both the blade dynamics and the flow field have been converged (Fig. 4-2). The converged unsteady upwash predicted on each of rotor blades (composed of the time-varying free stream, the companion blades and the unsteady wake) is then treated as an arbitrary gust. To find the lift response, each blade is segmented in the spanwise direction and each segment is treated as a two dimensional flat plate airfoil. The Kussner function is used with the Duhamel superposition integral to evaluate the loading response of the airfoil to this simplified gust problem. The basic transfer function approach assumes a two dimensional linear wake extending far downstream of the airfoil. However, to approximate the effect of the skewed helical wake of a rotor blade, which folds back on itself rather than extending to infinity, adjustments were made to the analysis being used that effectively truncated the wake at a finite distance downstream of the blade. Both the amplitude of the pressure response and the nondimensional time were corrected for compressibility in the spirit of Prandtl-Glauert. This approach clearly requires many approximations, but it does provide a consistent estimate of the unsteady surface pressure distribution on the rotor blades suitable for direct input to WOPWOP.

This method for determining the surface airloads distribution on the rotor blade is sufficient for demonstrating the feasibility of the transfer function approach to helicopter rotor aeroacoustic analysis. As it was discussed in Reference 26, calculations thus performed can provide some physical insight into the qualitative sensitivity of the predicted loading noise to selective input parameters and so help define some issues of interest for follow-on efforts. However, given the many approximations inherent in the present approach, it is not considered appropriate for the correlation of the acoustic predictions quantitatively with experimental data. It is recognized that substantial advances in the evaluation of the distributed surface loadings of the rotor blades have to be achieved before such correlation can be made with hope of success. Among the important issues to be addressed in improving this mode is the fact that the current analysis is based on an inviscid calculation and viscous shear stresses experienced on the blade surface have been neglected in the airloads evaluation. In addition, effects of three-dimensionality are in general of considerable importance in computing surface airloads, especially at the blade tip, and thus a transfer function with explicit representation of finite aspect ratio effects must be developed. Finally, efficient prediction of wake-induced inflow with high temporal resolution is also required. Such issues define some of the major challenges to be faced in converting the present analysis to a comprehensive analysis of rotor acoustics.

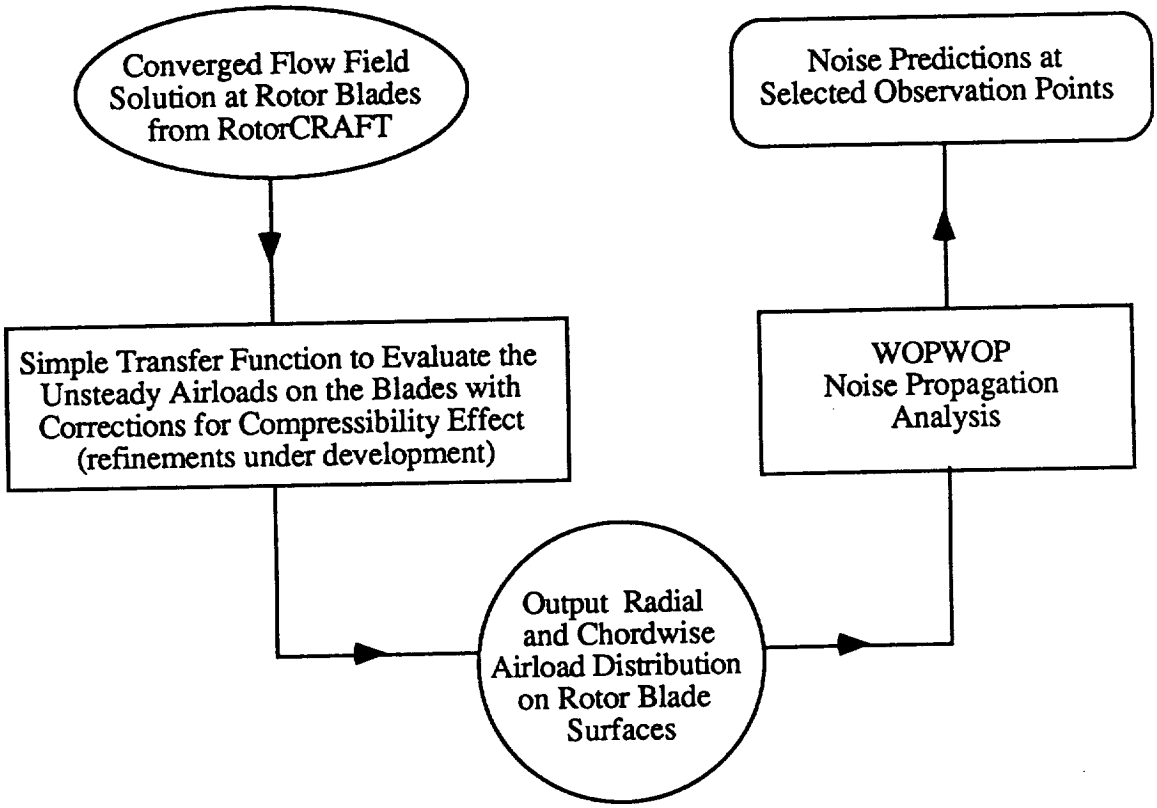

Figure 4-2. Implementation of the preliminary interface between RotorCRAFT and WOPWOP for the analysis of rotor noise predictions.

5. DATA CORRELATION STUDIES

Several data correlation studies using the baseline RotorCRAFT code were carried out as part of the development of the Mod 0.0 version of the code (Ref. 2). These calculations focused almost exclusively on steady and unsteady aerodynamic loading, though limited correlation of wind tunnel data on rotor flapping at low speed was also conducted. For the present effort, blade stress and hub load computations were of primary interest.

5.1 Blade Stress Calculations

One convenient and widely used source of blade stress data is the data base from the H-34 flight tests described in Reference 28. The correlation studies undertaken here will focus on examining flight conditions from that test. Undertaking blade stress calculations first requires the selection of mass and stiffness properties for the blade. Reference 28 did not contain this information, but it was assumed that the documentation of the H-34 blades used in the wind tunnel test in Reference 29 could be used. The blade structural calculations in RotorCRAFT require that this information be input in the form of radial distributions of the following quantities: Young's modulus and shear modulus; cross-sectional area; offset of the cross-sectional area centroid from the elastic axis; second moment of area about elastic axis; St. Venant's torsion constant for the section; angle between the local elastic axis and global spanwise axis; torsion/bending warping coefficients; mass per unit length; sectional center of mass offsets from the elastic axis; moments of inertia per unit length; and the cross product of inertia at each section. Detailed discussion of the input requirements for the RotorCRAFT structural properties file are given in Reference 15.

One of the important considerations in the analysis of blade stress using the RotorCRAFT analysis (or any comparable finite element analysis) is appropriate selection of the number and sizing of the elements used to discretize the blade. As noted above, the structural model consists of beam elements with fourteen degrees of freedom. Numerical experimentation with the H-34 configuration indicated that ten elements were sufficient to resolve the structural deformation for the purposes of blade stress calculations. More refined input files with as many as nineteen elements were prepared and used as input, but the results were found to be negligibly different from the ten-element cases discussed below.

The stress calculation procedures described in Section 3 above require the selection of a point of evaluation for the bending stress, described by a radial position and a vertical displacement from the blade's elastic axis. In the beam-rod approximation used in the present structural model, this corresponds to finding the stress in particular fibers at specified distances away from the elastic axis. The net stress experienced at a particular radial station can be found by differencing the stress computed at measurement points placed above and below the elastic axis; this differencing serves to subtract out the large mean stress component due to rotational effects, leaving an unsteady component attributable to aerodynamic loading and structural deflection.

The primary case of interest here is the advance ratio 0.29 case from Reference 28. Figure 5-1 shows a comparison of the total unsteady bending stress computed at r/R=0.65 with the measured value. There is some phase error in the first two quadrants, but the agreement is on the whole quite close. Of more general interest, however, is the vibratory blade stress, i.e. the components at 3P and higher for this four-bladed rotor. Recent work by Bousman (Ref. 30) involved general characterization of blade stress measurements across a wide range of rotor configurations, including the H-34 test examined here. The results quoted there indicated that the flapwise vibratory stress response of a variety of blades including the H-34 was dominated by a 3P component. Figure 5-2 shows this behavior for several different rotors, while Figure 5-3 features a surface plot of such response, drawn

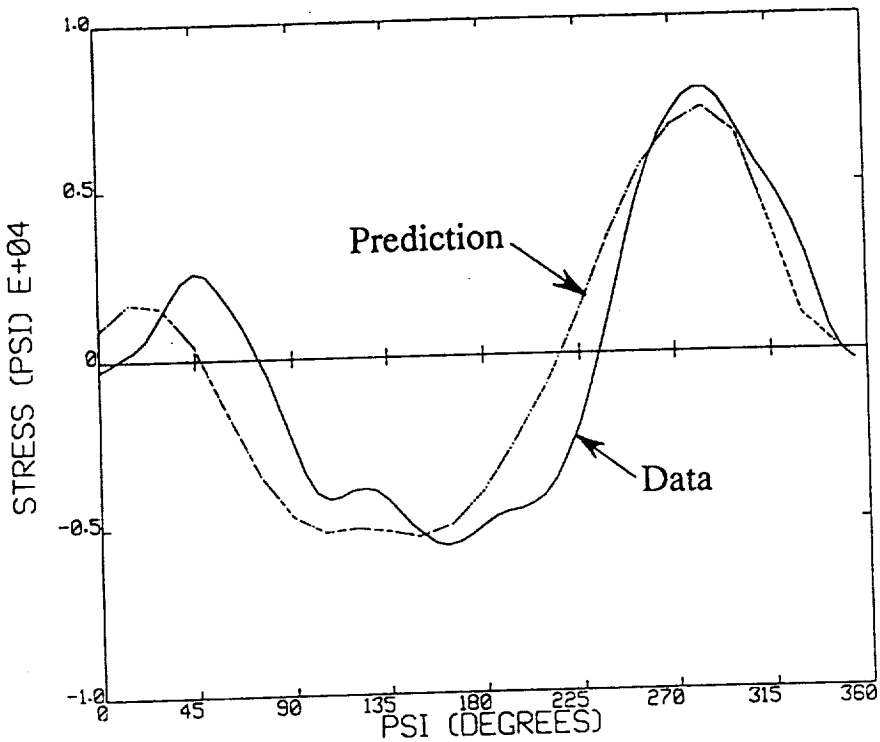

Figure 5-1. Total unsteady (harmonics 1-10) blade bending stress for the H-34 at advance ratio 0.29 .

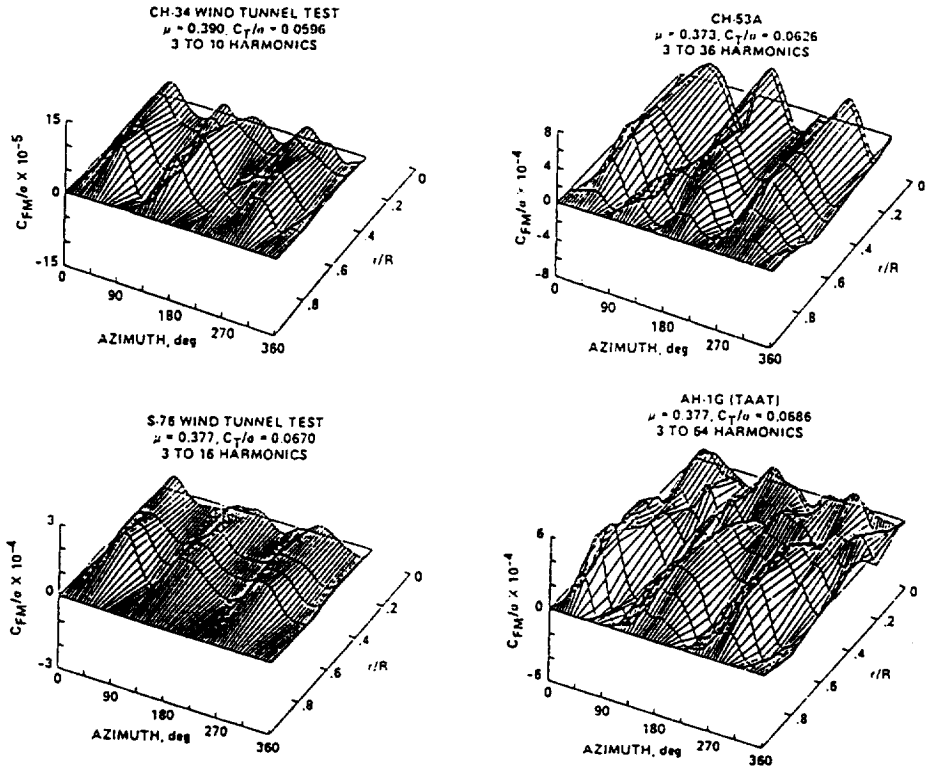

Figure 5-2. General trends in bending stress data for four rotors in high speed flight (from Ref. 28).

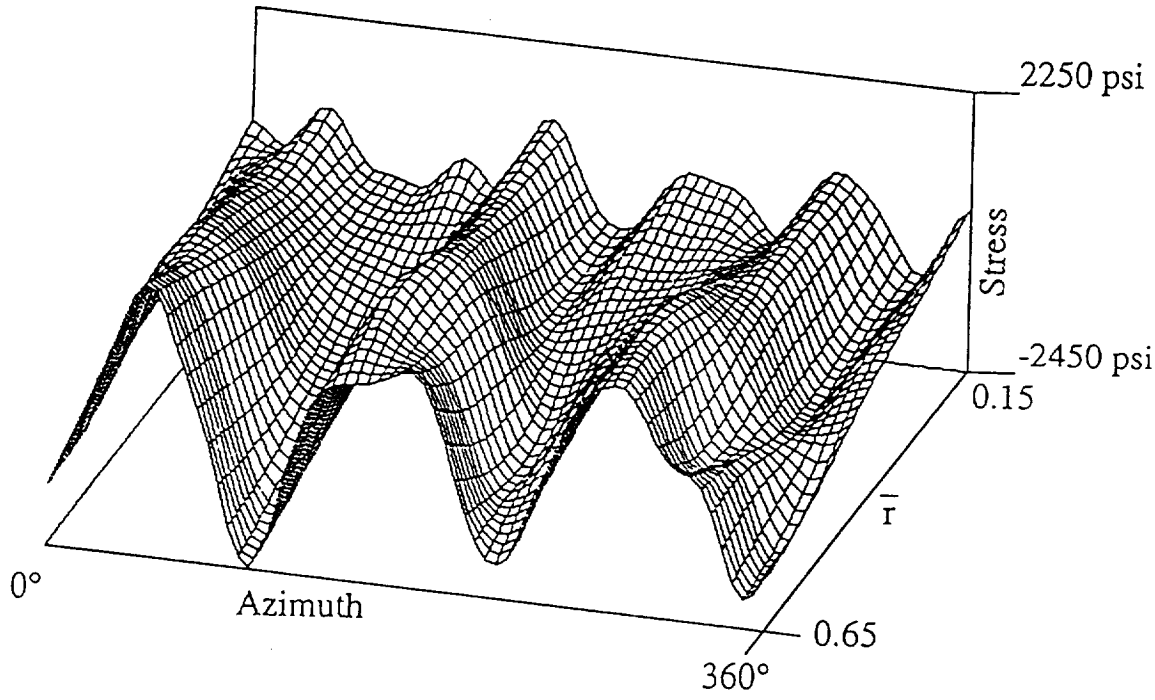

Figure 5-3. Surface plot of harmonics 3-5 of measured blade bending stress for the H-34 at advance ratio 0.29 (from Ref. 26).

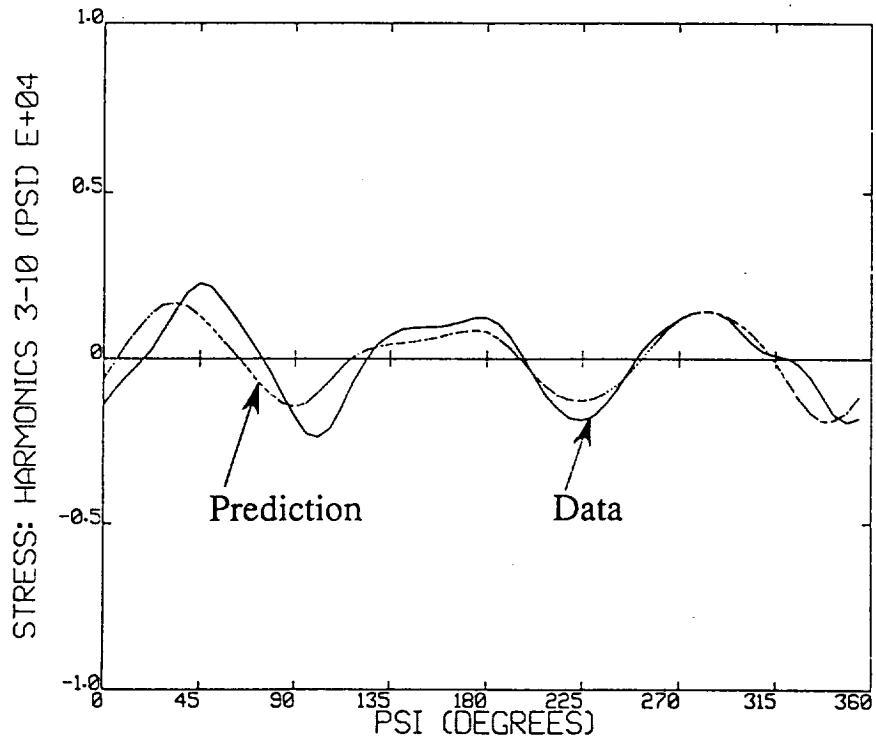

Figure 5-4. Vibratory (harmonics 3-10) blade bending stress for the H-34 at advance ratio 0.29 : r/R = 0.65 .

from the data in Reference 28. Figures 5-4 to 5-6 show the predicted levels of stress for harmonic components from 3P to 10P. All the results show good qualitative correlations, with the levels of response being particularly well predicted at the stations r/R=0.575 and 0.65. The results farther inboard tend to underpredict the level of stress response, particularly in the first quadrant.

5.2 Hub Load Calculations

As noted in Section 1, the experimental results reported in Reference 1 indicate considerable promise in the application of higher harmonic pitch control for noise reduction. Several of the test cases described in Reference 1 were examined using RotorCRAFT (Mod 1.0) to assess the correlation between the predicted and measured loads. The experimental rotor was tested in the Transonic Dynamics Tunnel (TDT) at NASA/Langley and will be referred to hereafter as the TDT rotor. The rotor radius was 4.58 ft. and its chord was constant over the span at a value of 0.35 ft. The blades were untwisted, and the cross-sectional properties were supplied by NASA personnel and suitably arranged for input into RotorCRAFT (Mod 1.0). The rotor was tested in heavy gas (freon) so that Mach-scale tests could be conducted at reduced tip speeds. The tip speed used in the tests in Reference 1 was 311 fps, corresponding to a rotor rotation frequency of 68 rad/sec. The tests to be examined in detail here are four flight conditions from those documented in Reference 1; these particular cases were chosen since they 'bracket' the advance ratio and shaft angle range considered. The four flight conditions are: advance ratio 0.166 at shaft angle of attack +6.0°, (designated 'Case A', corresponding to Figure 17a of Reference 1); advance ratio 0.30 at shaft angle +2.0° (Case C); advance ratio 0.166 at shaft angle 0° (Case G); and advance ratio 0.3 at shaft angle -4.0° (Case I). In each case the rotor thrust coefficient was 0.0050.

The first step in this correlation study was to compute the modal properties of the blade using the finite element structural analysis in the RotorCRAFT code, as described in Reference 2. The predicted modal frequencies for the first three out-of-plane bending modes were 1.05P, 2.62P, and 4.90P, while in-plane frequencies were computed to be 0.31P (rigid lag) and 4.12P (first elastic lag). The corresponding frequencies predicted by CAMRAD were 1.04P, 2.61P, 4.82P, 0.29P and 4.18P, respectively (Ref. 31). The modal frequency calculations also predicted that the first elastic torsion frequency is quite high (8.60P). Since the primary experimental data of interest is 4P hub loading, it appears unlikely that torsional deflection participates to any large degree in this response. RotorCRAFT (Mod 1.0) permits the user to select which elastic deflection modes are to be included in the analysis. It was determined that an appropriate numerical model featured three out-of-plane bending modes (rigid flapping and the first two elastic bending modes) as well as two in-plane modes (rigid lag and first elastic lag).

In addition to the specification of the blade's geometry and structural properties, the RotorCRAFT code requires the user to select a vortex lattice configuration for the blade as well as a wake model suitable to the flight condition. For all the calculations described below, the blade model uses a vortex lattice with 30 vortex quadrilaterals spanwise and one chordwise quad. For Case C and Case I, the calculations use a maximum of eighteen wake filaments trailing from Zone 1 and ten from Zone 2 (see Ref. 15 for definitions of these Zones), with one full turn of full-span CVC wake and one turn of free wake extensions in each case. For the relatively low speed calculations of Case A and Case G, a longer free wake was required, though the same number of filaments were trailed from the span. In each case, default selections for the vortex cores were made. It is possible that changes of one or more of these parameters may affect the results obtained below, though these selections were

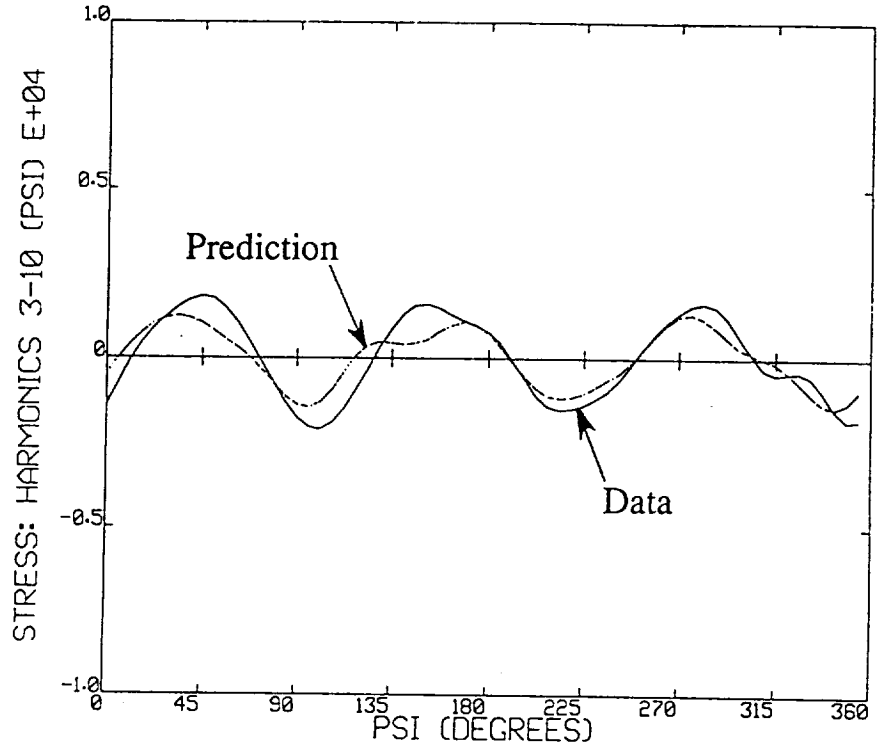

Figure 5-5. Vibratory (harmonics 3-10) blade bending stress for the H-34 at advance ratio 0.29 : r/R = 0.57 .

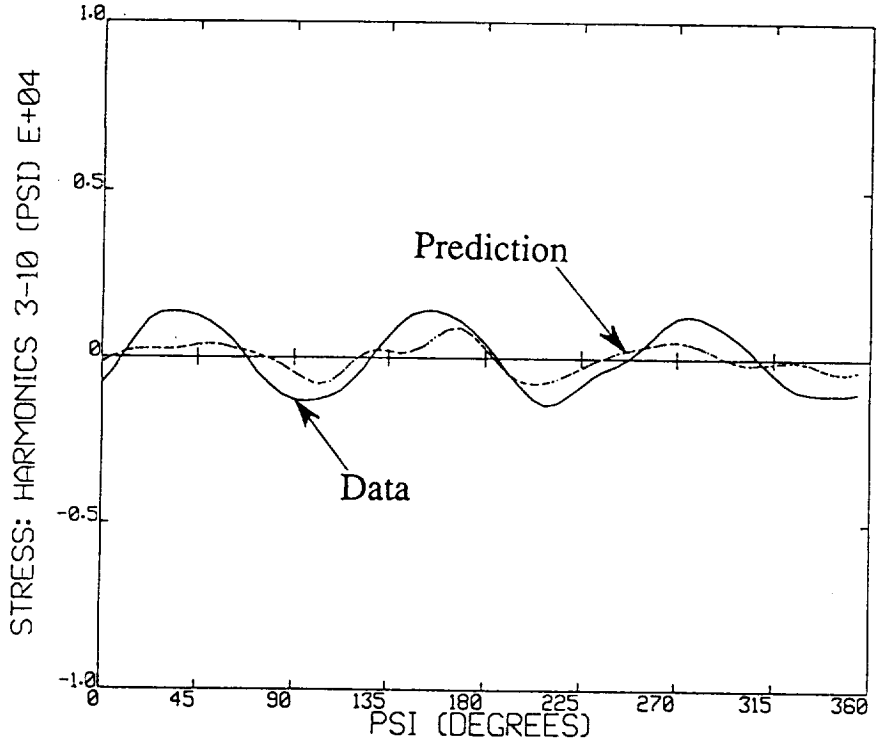

Figure 5-6. Vibratory (harmonics 3-10) blade bending stress for the H-34 at advance ratio 0.29 : r/R = 0.45 .

made on the basis of substantial numerical experimentation with other similar rotor configurations.

Figure 5-7 shows a snapshot of wake geometry in Case I both before and after the application of 4P higher harmonic pitch. The change in wake structure is quite marked; the presence of closed circles in the wake indicate the appearance and disappearance of loading peaks due to the time-varying pitch. Since the flow field produced by the filament wake is correspondingly altered, this illustrates one of the advantages of using the refined CVC wake model for this type of calculation.

Reference 1 specified the higher harmonic pitch input used in each case. As noted above, RotorCRAFT (Mod 1.0) can take as input arbitrary periodic pitch time histories including higher harmonic forms such as :

$$\theta(\psi) = \theta_0 + \theta_{1c}\cos\psi + \theta_{1s}\sin\psi + \ldots + \theta_{nc}\cos n\psi + \theta_{ns}\sin n\psi + \ldots \qquad (5.1)$$

For these correlation calculations, the steady and first harmonic pitch inputs were chosen to trim the rotor to zero first harmonic flapping at the desired thrust coefficient. All other harmonic components were set to zero, except the 4P terms. Reference 1 specified these inputs in terms of a magnitude θ_C and a phase angle ψ_c. These were transformed into the required components of θ using

$$\theta_{4c} = \theta_c \cos 4\psi_c \qquad \text{and} \qquad \theta_{4s} = \theta_c \sin 4\psi_c$$

These inputs replicate the 4P collective pitch inputs used in the test, which featured amplitudes of $\theta_c = -0.6°$ and $\theta_c = -1.2°$. The value of the phase angle ψ_c ranged from 0° to 90° for each of the flight conditions examined.

Before calculating the vibratory load response to higher harmonic control inputs (HHC), the prediction of levels of vertical hub force with no HHC was first considered. The data presented in Figure 5-8 were drawn from Figure 17 of Reference 1. Except for Case C, the load magnitudes predicted by RotorCRAFT (Mod 1.0) without HHC agree with the measured data to within 10%. Therefore, any discrepancies greater than this that are encountered in the comparisons that follow are assumed to be associated with the effect of modeling higher harmonic control inputs.

The tests described in Reference 1 were performed on a non-scaled rotor hub that generated substantial inertial vibratory load when subjected to the 4P higher harmonic pitch input. The quantities measured in the test were the forces and moments transmitted to the stationary reference frame. For comparison with RotorCRAFT (Mod 1.0) predictions, the inertial forces associated with the swashplate motion were estimated and subtracted from the total forces obtained during the test. The aerodynamic and aeroelastic force contributions remaining are equivalent to those calculated by the RotorCRAFT (Mod 1.0) code. The hub force data presented in Figures 5-9 and 5-10 were obtained from the following formula

$$(F_{4P})_{aero} = (F_{4P})_{total} - F_i(\ddot{\theta}_{4P})_{HHC} \qquad (5.1)$$

where F_i is the magnitude of the inertial force associated with the swashplate motion. The vector sense of the forces here represents the sin 4ψ and cos 4ψ components; the inertial force is in phase with the pitch control acceleration. A value of $F_i = 44.74$ lbs was used for the current analysis (Ref. 32).

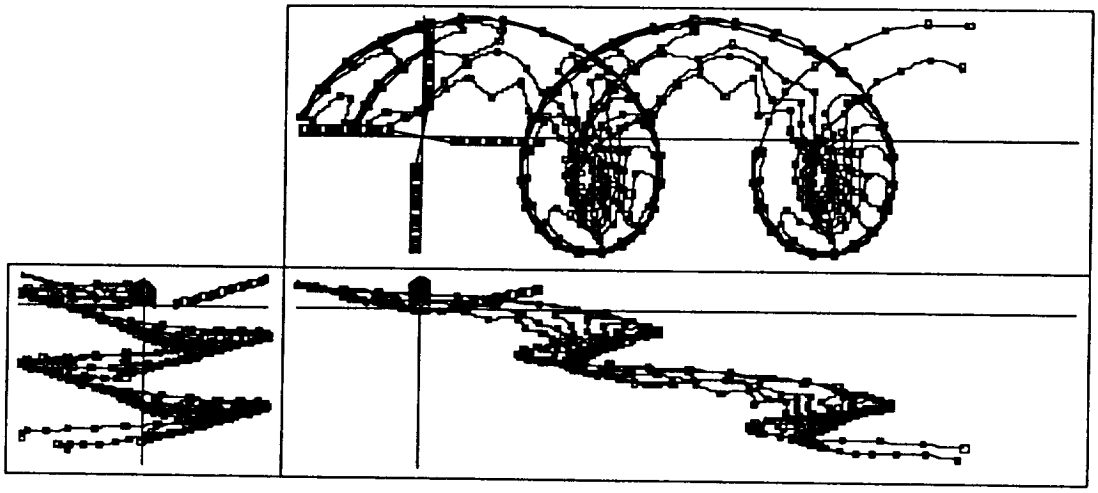

a) With no HHC input

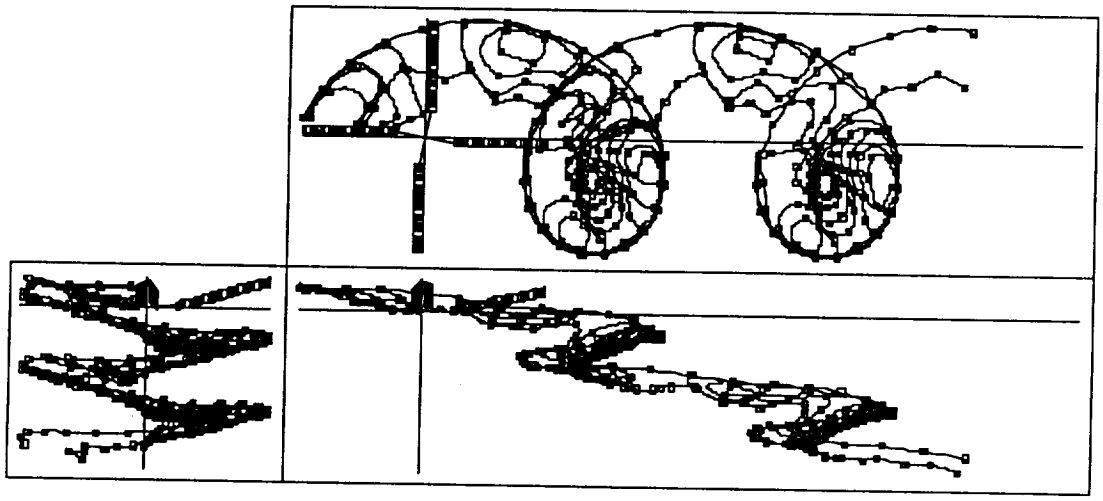

b) With HHC input

Figure 5-7. Wake geometry for $\mu = 0.3$, $\alpha_S = -4.0°$ with no HHC pitch input (top) and with HHC pitch input ($\theta_C = -1.2°$, $\Psi_C = 0°$) (bottom). (Vertical scale expanded by a factor of 5.0 .)

14. Bliss, D.B., Teske, M.E., and Quackenbush, T.R.: "A New Methodology for Free Wake Analysis Using Curved Vortex Elements", NASA CR 3958, 1987.

15. Wachspress, D.A., Quackenbush, T.R., and Boschitsch, A.H.: "RotorCRAFT (Mod 1.0) Users Manual", Continuum Dynamics, Inc., Technical Note 91-12, October 1991.

16. Quackenbush, T.R., Bliss, D.B.: "Free Wake Flow Field Calculations for Rotorcraft Interactional Aerodynamics", Vertica Vol. 14, No.3, pp. 313-327, 1990.

17. Quackenbush, T.R., Bliss, D.B., Lam, C-M.G., Katz, A.: "New Vortex/Surface Interaction Methods for the Prediction of Wake-Induced Airframe Loads", proceedings of the 46th Annual Forum of the American Helicopter Society, Washington DC, May 1990.

18. Falkner. V. M.: "The Calculation of Aerodynamic Loading on Surfaces of Any Shape", Aeronautical Research Council, R&M 1910, August 1943.

19. Rubbert, P.E.: "Theoretical Characteristics of Arbitrary Wings by a Nonplanar Vortex Lattice Method", Report 06-9244, The Boeing Company, Seattle, WA., 1964.

20. Margason, R.J. and Lamar, J.E.: "Vortex Lattice FORTRAN Program for Estimating Subsonic Aerodynamic Characteristics of Complex Planforms", NASA TN-D 6142, 1971.

21. Quackenbush, T.R., et al.: "Free Wake Analysis of Hovering Performance Using a New Influence Coefficient Method", NASA CR 4309, July 1990.

22. Chiu, Y.D.: "Convergence of Discrete-Vortex Induced-Flow Calculations by Optimum Choice of Mesh", Ph.D. Thesis, Georgia Institute of Technology, School of Aerospace Engineering, August 1988.

23. Celi, R. & Friedmann, P. P., "Aeroelastic Modeling of Swept Tip Rotor Blades Using Finite Elements", Journal of the AHS, Volume 33, Number. 2, pp. 43-52., April 1988.

24. Bathe, K.J.: *Finite Element Procedures in Engineering Analysis*, Prentice-Hall, Inc., 1982.

25. Quackenbush, T.R. and Bliss, D.B.: "High Resolution Flow Field Prediction for Tail Rotor Aeroacoustics", Proceedings of the 45th Annual Forum of the AHS, May 1989.

26. Quackenbush, T.R., Bliss, D.B., Bilanin, A.J., Lam, C-M.G.: "General Flow Field Analysis Methods for Helicopter Rotor Aeroacoustics", CDI Report 90-04, August 1990

27. Brentner, K.S., "Prediction of Helicopter Rotor Discrete Frequency Noise", NASA TM-87721, October 1986.

28. Scheiman, J.: "A Tabulation of Helicopter Rotor-Blade Differential Pressures, Stresses, and Motions Measured in Flight", NASA TM-X 952, March 1964.

29. Rabbott, Jr., J.P., Lizak, A.A. and Paglino, V.M.: "A Presentation of Measured and Calculated Full-Scale Rotor Blade Aerodynamic and Structural Loads",

30. Bousman, W.G.: "The Response of Helicopter Rotors to Vibratory Airload", Proceedings of the AHS national Specialists' Meeting on Rotorcraft Dynamics, Dallas, TX, November 1989.

31. Boyd, D., Private Communication, November 1990.

32. Booth, E.R., Private Communication, November 1991.

33. Brooks, T.F., et. al.: "Rotor HHC Acoustics Study in the DNW to Reduce BVI Impulsive Noise", Proceedings of the AHS/RAeS International Technical Specialists' Meeting on Rotorcraft Acoustics, Philadelphia, PA, October 1991.

REPORT DOCUMENTATION PAGE

Form Approved
OMB No. 0704-0188

1. AGENCY USE ONLY (Leave blank)	2. REPORT DATE	3. REPORT TYPE AND DATES COVERED
	April 1992	Contractor Report

4. TITLE AND SUBTITLE
Analysis of Rotor Vibratory Loads Using Higher Harmonic Pitch Control

5. FUNDING NUMBERS
NAS1-19160
WU 532-06-37

6. AUTHOR(S)
Todd R. Quackenbush, Donald B. Bliss, Alexander H. Boschitsch, and Daniel A. Wachspress

7. PERFORMING ORGANIZATION NAME(S) AND ADDRESS(ES)
Continuum Dynamics, Inc.
P.O. Box 3073
Princeton, New Jersey 08543

8. PERFORMING ORGANIZATION REPORT NUMBER
C.D.I. Report No. 91-02

9. SPONSORING/MONITORING AGENCY NAME(S) AND ADDRESS(ES)
National Aeronautics and Space Administration
Langley Research Center
Hampton, Virginia 23665-5225

10. SPONSORING/MONITORING AGENCY REPORT NUMBER
NASA CR-189591

11. SUPPLEMENTARY NOTES
Langley Technical Monitor: T.F. Brooks

12a. DISTRIBUTION/AVAILABILITY STATEMENT
Unclassified - Unlimited
Subject Category 71

12b. DISTRIBUTION CODE

13. ABSTRACT *(Maximum 200 words)*

Experimental studies of isolated rotors in forward flight have indicated that higher harmonic pitch control can reduce rotor noise. These tests also show that such pitch inputs can generate substantial vibratory loads. This report summarizes the modification of the RotorCRAFT (Computation of Rotor Aerodynamics in Forward flighT) analysis of isolated rotors to study the vibratory loading generated by high frequency pitch inputs. The original RotorCRAFT code was developed for use in the computation of such loading, and uses a highly refined rotor wake model to facilitate this task. The extended version of RotorCRAFT incorporates a variety of new features including: arbitrary periodic root pitch control; computation of blade stresses and hub loads; improved modeling of near wake unsteady effects; and preliminary implementation of a coupled prediction of rotor airloads and noise. Correlation studies are carried out with existing blade stress and vibratory hub load data to assess the performance of the extended code.

14. SUBJECT TERMS	15. NUMBER OF PAGES
Higher harmonic pitch; Vibratory loading; Rotor noise	59
	16. PRICE CODE

17. SECURITY CLASSIFICATION OF REPORT	18. SECURITY CLASSIFICATION OF THIS PAGE	19. SECURITY CLASSIFICATION OF ABSTRACT	20. LIMITATION OF ABSTR
UNCLASSIFIED	UNCLASSIFIED	UNCLASSIFIED	UL